THE ASTROPHYSICAL JOURNAL, 429:300–318, 1994 July 1

SN 1993J: A TYPE IIb SUPERNOVA[1]

S. E. WOOSLEY,[2,3] RONALD G. EASTMAN,[2] THOMAS A. WEAVER,[3] AND PHILIP A. PINTO[4]

Received 1993 May 20; accepted 1993 December 23

ABSTRACT

The evolution of the bright Type II supernova discovered last year in M81, SN 1993J, is consistent with that expected for the explosion of a star which on the main sequence had a mass of 13–16 $M_\odot$ but which, owing to mass exchange with a binary companion (a initially $\sim$3–5 AU, depending upon the actual presupernova radius and the masses of the two stars) lost almost all of its hydrogen-rich envelope during late helium burning. At the time of explosion, the helium core mass was 4.0 ± 0.5 $M_\odot$ and the hydrogen envelope, 0.20 ± 0.05 $M_\odot$. The envelope was helium and nitrogen-rich (carbon-deficient) and the radius of the star, $4 \pm 1 \times 10^{13}$ cm. The luminosity of the presupernova star was $3 \pm 1 \times 10^{38}$ ergs s^{-1}, with the companion star contributing an additional $\sim 10^{38}$ ergs s^{-1}. The star may have been a pulsating variable at the time of the explosion. For an explosion energy near 10^{51} ergs (KE at infinity) and an assumed distance of 3.3 Mpc, a mass of ^{56}Ni in the range 0.07 ± 0.01 $M_\odot$ was produced and ejected. This prescription gives a light curve which compares favorably with the bolometric observations. Color photometry is more restrictive and requires a model in which the hydrogen-envelope mass is low and the mixing of hydrogen inward has been small, but in which appreciable ^{56}Ni has been mixed outward into the helium and heavy-element core. It is possible to obtain good agreement with B and V light curves during the first 50 days, but later photometry, especially in bands other than B and V, will require a non–LTE spectral calculation for comparison. Based upon our model, we predict a flux of $\sim 10^{-5}$ (3.3 Mpc/D)^2 photons cm^{-2} s^{-1} in the 847 keV line of ^{56}Co at peak during 1993 August. It may be easier to detect the Comptonized continuum which peaks at a few times 10^{-4} photons s^{-1} cm^{-2} MeV^{-1} at 40 keV a few months after the explosion (though neither of these signals were, or should have been, detected by the *Compton Gamma-Ray Observatory*). The presupernova star was filling its Roche lobe at the time of the explosion and thus its envelope was highly deformed (about 3:2). The companion star is presently embedded in the supernova, but should become visible at age 3 yr (perhaps earlier in the ultraviolet) when the supernova has faded below 10^{38} ergs s^{-1}. Indeed, if "kicks" have not played an important role, it is still bound to the neutron star.

Subject headings: galaxies: individual (M81) — supernovae: individual (SN 1993J)

1. INTRODUCTION

As this paper was begun in 1993 May, SN 1993J was 6 weeks old and it was already clear that it differed from a normal Type II "plateau" (IIp) supernova. The evolution was unusually rapid, the light curve in all bands nonmonotonic, and, following a strong secondary peak, the bolometric emission was gradually settling onto a radioactive "tail." There were also spectroscopic indications that the supernova was making the transition from Type II to Type Ib (Filippenko & Matheson 1993). This transformation and some of its implications have now been well described by Filippenko, Matheson, & Ho (1993) and bolometric light curves have been published by Schmidt et al. (1993), Ray, Singh, & Suturia (1993), and Richmond et al. (1993).

Over the next several months, as we completed our work, numerous preprints arrived (Nomoto et al. 1993; Shigeyama et al. 1994; Suzuki et al. 1993; Hashimoto, Iwamoto, & Nomoto 1993; Höflich, Langer, & Duschinger 1993; Podsiadlowski et al. 1993; Wheeler et al. 1993; Bartunov et al. 1994; Baron et al. 1993; Ray et al. 1993; Schmidt et al. 1993; Swartz et al. 1993; Utrobin 1993), all arriving at the same general conclusion—that SN 1993J was the explosion of a massive star (10–20, or maybe even 35 $M_\odot$) that had lost most of its hydrogen envelope. An excellent review of this early work can be found in Wheeler & Filippenko (1994). All but Höflich et al. invoked binary mass exchange as the explanation of the low-mass envelope and many noted the similarity to Type Ib light curves. Most papers concentrated on modeling the bolometric light curve of Schmidt et al. (1993), but also derived interesting limits on the mass of ^{56}Ni synthesized, the mass of the star that exploded, its distance, the mass of its hydrogen envelope (quite diverse values were deduced), and other properties.

Although our results have been obtained independently, the work reported here reaches many similar conclusions. We shall concentrate on our new results, but emphasize, where appropriate, the relation to other work. Unlike the other papers, we attempt a comprehensive model for SN 1993J, one that begins on the main sequence and follows the evolution in detail through the first year of the supernova.

As we shall see, SN 1993J may properly be termed a Type IIb supernova—Type II because prominent lines of hydrogen were apparent in the spectrum near peak and subclass b to denote the spectroscopic and photometric similarity to Type Ib supernovae. We prefer this designation to the term "stripped supernova" employed by Podsiadlowski et al. (1993) and Hsu et al. (1991) because, though the latter is physically descriptive, it refers to a model and not an observational class.

Ever since SN 1987A, the idea of a Type II supernova

[1] Lick Observatory Bulletin No. B1283.

[2] University of California Observatories/Lick Observatory, Board of Studies in Astronomy and Astrophysics, University of California, Santa Cruz, Santa Cruz, CA 95064.

[3] General Physics Division, University of California, Lawrence Livermore National Laboratory, Livermore, CA 94550.

[4] Department of Astronomy, University of Arizona, Tucson, AZ 85721.

powered at visual peak by radioactivity has not been new. Indeed, following SN 1987A, but before it became apparent that the blue progenitor had exploded with most of its envelope intact (e.g., Arnett et al. 1989), many models were suggested based upon the premise that the progenitor star had lost most, but not all, of its hydrogen envelope and was thus on the way to becoming a Wolf-Rayet star. It was within this context that Woosley, Pinto, & Ensman (1988) coined the term "Type IIb" to describe such a model because of the similarities it bears to massive star models for Type Ib supernovae (e.g., Ensman & Woosley 1988). However, all models for SN 1987A were constrained to have the small radius and large envelope mass of the blue progenitor Sk 202-69 and are thus inappropriate to SN 1993J. Woosley (1991) first calculated the light curve for the red supergiant version of a massive star that had lost most of its hydrogen envelope—a 6 $M_\odot$ helium core that exploded with a 1 $M_\odot$ hydrogen envelope in place and a radius of 1.7×10^{13} cm. Two models were calculated, one producing 0.2 $M_\odot$ of ^{56}Ni and another, 0.07 $M_\odot$. This latter model bears a striking similarity to what has been observed in SN 1993J and is, qualitatively, a good description of this event. However, as we shall see shortly, the envelope mass in SN 1993J was much smaller, the helium core also somewhat smaller, the radius much larger, and, in this case, the mass loss is almost certainly a consequence of mass exchange with a binary companion.

Observationally, SN 1993J is also similar to another famous Type IIb supernova—SN 1987K (Filippenko 1988). This supernova was born Type II, with a light curve that, though sparsely sampled, resembles SN 1993J. Later in its evolution, SN 1987K became spectroscopically very similar to Type Ib supernovae. The same has by now happened to SN 1993J.

The specific model we have in mind for SN 1993J is the explosion of a star which, on the main sequence, had mass in the range 13–16 $M_\odot$, but which was in a binary system with a star of uncertain (though obviously smaller) initial mass separated by several AU. Toward the end of helium burning, as the supernova progenitor swelled to become a fully developed red supergiant, it began to transfer mass to its companion. For a short time, this transfer was very rapid and the envelope of the primary decreased rapidly in mass from about 10 $M_\odot$ to ~ 1 $M_\odot$ (§ 2; see also Podsiadlowski, Joss, & Hsu 1992). The envelope mass continued to decline, but more slowly as the core of the star depleted helium. The transition to carbon burning and more advanced stages led to a final increase in luminosity (coming from the helium shell) and mass transfer just prior to the explosion that further reduced the envelope mass to about 0.2 $M_\odot$. The progenitor was still filling its Roche lobe when the explosion occurred, and most of the volume of the presupernova star was filled with helium-rich, low-density envelope. It was the release, by recombination, of the energy deposited in this envelope by the shock that gave rise to the early emission and first peak of the light curve. The decay of 0.07 $M_\odot$ of ^{56}Co produced in the explosion gave the second peak and is currently powering the supernova.

In the next section we discuss the evolution of the progenitor star in some detail. Lacking a firm fix on the mass of the presupernova star and knowing even less about the mass of the companion and its orbit, in turns out that SN 1993J lacks a unique solution, but has instead a family of solutions that give about the same envelope mass and presupernova radius. The free parameters are the mass of the companion, the initial orbital separation, and how conservative (or nonconservative) the mass transfer process was. Subsequent sections explore the explosion of the star, the light curve, both bolometric and in various wave bands, and present the expected γ-ray light curve of the supernova. Section 7 gives our conclusions.

2. PRESUPERNOVA MODELS AND EXPLOSION

2.1. *Overview*

The absolute magnitude of the progenitor of SN 1993J was initially estimated to be roughly -7.5 (modulo an uncertain reddening correction and distance modulus, contamination by companion stars, and possible variability; Perlmuter 1993; Humphreys et al. 1993; Magnier et al. 1993; Blakeslee & Tonry 1993). This corresponds to a luminosity of about 3×10^{38} ergs s^{-1}. Filippenko et al. (1993) estimated the luminosity of the progenitor *including any bound companion*, but no other nearby stars, to be in the range 2.5–4 $\times 10^{38}$ ergs s^{-1}. Even for single stars, this would rule out progenitors more massive than about 17 $M_\odot$ (Table 1). For a companion luminosity of $\sim 10^{38}$ ergs s^{-1}, the limit drops to 15 $M_\odot$. More recently Aldering, Humphreys, & Richmond (1993) have estimated the bolometric magnitude of the progenitor star, corrected for the presence of a binary companion, to be -7.8, or $L = 4.0 \times 10^{38}$ ergs s^{-1}, appropriate for a star of approximately 16 $M_\odot$ (Table 1). This defines the largest stars to be considered in our study. The lowest mass to be considered, 11 $M_\odot$, is set by the need to synthesize appreciable ^{56}Ni in the explosion, though the luminosity limits discussed above suggest that the star was more massive than 11 $M_\odot$.

Such stars are not expected to lose most of their envelopes by radiatively driven mass loss (e.g., Chiosi & Maeder 1986). Even if they did, it would be unlikely that a star would explode just as its envelope mass declined to $\sim 1\%$ of its initial value. Further, unless the explosion mechanism was able to deliver very much more than 10^{51} ergs, the expansion of a 30 $M_\odot$ star, say, even without its hydrogen envelope, would be too slow and would give a light curve with a second maximum that occurred later and declined slower than SN 1993J (Ensman & Woosley 1988). Henceforth, we shall presume that the progenitor of SN 1993J lost its envelope due to mass exchange with a binary companion. We shall find that this naturally leaves a ~ 0.2 $M_\odot$ of envelope at the time of explosion, precisely what is needed to explain the observations.

What were the properties of this binary and how do they relate to what was observed? Certainly the initial mass of the presupernova star was important as it sets the helium core mass, a critical parameter for the explosion hydrodynamics, the nucleosynthesis, and the light curve. Another very important property of the binary was the Roche radius of the presu-

TABLE 1

PRESUPERNOVA MODELS WITHOUT MASS LOSS

Mass	$R_{\rm pre\ SN}$ (10^{13} cm)	M_α[a] ($M_\odot$)	$L_{\rm pre\ SN}$ (10^{38} ergs s^{-1})	$L_{\rm ZAMS}$ (10^{38} ergs s^{-1})
11.....	2.24	2.86	1.54	0.45
13.....	2.80	3.57	2.35	0.69
15.....	3.34	4.34	3.27	0.84
18.....	4.12	5.54	4.95	1.43
20.....	4.87	6.69	7.76	1.78
22.....	5.19	7.59	8.00	2.25
25.....	5.91	9.11	10.3	3.09

[a] M_α is the size of the helium core; specifically that location where the hydrogen mass fraction is 0.01.

pernova star at the time of its explosion. If this radius were smaller than about 2 AU (somewhat larger values will be preferred), the supernova, whose progenitor is constrained to fit in this volume, would have had too small an envelope, both in mass and radius, to power the first peak of the light curve. Conversely, a radius of more than a few AU would have given a first peak that was overly broad, occurred too late, and was too bright (here a larger final radius would also imply a larger envelope mass). Supernova 1993J must therefore have happened in a system that had the right final orbital parameters to give a Roche radius between 2 and several AU. Moreover, the *initial* separation must have been such as to allow mass transfer to occur in the first place.

Ignoring for the moment the unusual case of SN 1987A and other stars that end their lives as blue supergiants, a presupernova star has its largest radius and highest luminosity just as it explodes. This luminosity comes entirely from the helium burning shell and, for a pulsationally stable star, is determined entirely by the characteristics of the helium core, mainly its mass and the size of the carbon-oxygen core within. Table 1 gives the properties of some main-sequence and presupernova stars evolved without mass loss. These particular models are taken from Weaver & Woosley (1994) but are very similar in structure and composition to another recent series of models (Weaver & Woosley 1993). For present purposes, they differ only in having employed finer zoning and shorter time steps.

Figure 1 shows for 11 and 15 $M_\odot$ stars the orbital separation as a function of companion mass for which $R_R = R_F$, where R_F is the presupernova radius and the Roche radius is given by Eggleton (1983)

$$\frac{R_R}{a} = \frac{0.49q^{2/3}}{0.6q^{2/3} + \ln(1 + q^{1/3})} . \quad (1)$$

Here R_R is the Roche radius of the mass-losing star; q is the ratio of the mass-donating star to that of the mass-accepting star; and a is their separtion. Figure 1 shows, for example, that a 15 $M_\odot$ star will be uninfluenced by a binary companion if the initial orbital separation exceeds 6 AU, even for the most massive allowed companions, and 4 AU for lightest allowed companions. Systems with larger separations could not have produced SN 1993J.

There is also a *minimum* initial separation that will allow the necessary red supergiant progenitor to exist without losing too much of its small remaining envelope. The calculation of this minimum value is not so straightforward as the maximum because it involves assumptions about the efficiency of mass transfer (how much of the mass lost by the primary ends up on the secondary) and the amount of angular momentum lost from the system. The transfer may be nonconservative, but for present purposes and simplicity of discussion we shall assume that it is conservative or very nearly so. We are interested only in the range of final Roche radii allowed for the progenitor, and relatively minor adjustments in the parameters can give the same result with nonconservative transfer. These adjustments for nonconservative transfer are straightforward and have been discussed by Podsiadlowski et al. (1992).

For mass transfer in which both mass and angular momentum are conserved, the separation evolves as $a \propto (M_1 M_2)^{-2}$ (Frank, King, & Raine 1992) and the final separation is given in terms of the initial separation, a_0, by

$$a_{\rm final} = a_0 \left(\frac{M_1^0 M_2^0}{M_\alpha} \right) (M_1^0 + M_2^0 - M_\alpha) , \quad (2)$$

where M_α, the helium core mass, is given in Table 1 and we have assumed that the mass of the final hydrogen envelope is small compared to M_α. Solving for a final Roche radius of 1 AU or 2 AU gives the lines in Figure 1. Physically, these are the initial separations that characterize the binary composed of the given two masses in order to end up with a Roche radius for the mass-donating component of the given value. For example, a 15 $M_\odot$ star born with a 10 $M_\odot$ companion and experiencing conservative transfer throughout its evolution will end up with a Roche radius of 2 AU if the initial separation is 2.8 AU. For this same system, initial separations smaller than 2 AU and larger than 5 AU are not probable, though nonconservative transfer can extend these limits somewhat. We shall find in subsequent sections that the final Roche radius of SN 1993J was not less than 2 AU. All these estimates assume spherical geometry which, as we shall see, is not quite correct.

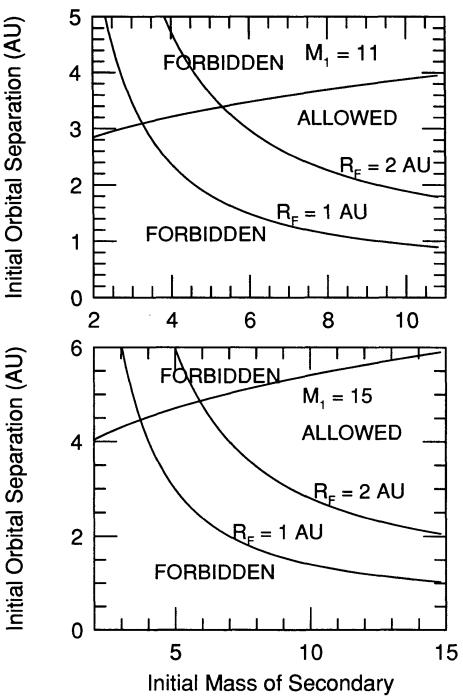

FIG. 1.—Combinations of initial binary orbital separation and companion mass that allow the formation of red supergiants with small hydrogen envelope masses. The top figure shows, for an 11 $M_\odot$ primary, "forbidden" regions of large separation, where mass exchange will never occur, and small separation where the presupernova radius, R_F, will have to be smaller than 1 (or 2) AU. Such small radii are incompatible with the light curve of SN 1993J. The allowed region is the roughly triangular area on the right-hand side below the gently upwardly sloping line and above the line $R_F = 2$ AU. The bottom figure shows similar restrictions on a 15 $M_\odot$ primary. Conservative mass transfer is assumed in both cases.

2.2. *Computer Code*

The stellar evolution code employed was KEPLER (Weaver, Zimmerman, & Woosley 1978; Weaver & Woosley 1993), suitably modified for mass loss. Mass loss was accomplished by steadily decreasing the mass of an arbitrary Lagrangian mass zone near the surface of the star. In practice, a zone below the surface of 0.005 times the current mass of the star was employed (e.g., 0.075 $M_\odot$ interior to the surface of a main-sequence 15 $M_\odot$ star). As the mass of this zone becomes small compared to its neighbors, the automatic rezoner, which con-

serves momentum and energy very well, reallocates the mass of the small zone and the zones above and below (three zones in total) into two new zones and the process continues. Adzoning keeps all relevant gradients smooth. The zoning, mass-loss rate, and time steps are such that the rezoned region remains in thermal equilibrium, i.e., the luminosity coming from deep in the star is not altered as it flows through this region. Composition external to the rezoned region is kept constant at a value equal to that immediately below the mass-losing region. This becomes important as the mass loss moves into a region where there is a hydrogen-helium gradient.

Our numerical prescription for mass loss incorporates both radiative loss (de Jager, Nieuwenhuijzen, & van der Hucht 1985, with constants as given by Chiosi & Maeder 1986) and mass transfer. The former turns out to be unimportant for the stars considered here except for cases when the rate of semiconvective diffusion is taken to be very small. Binary transfer is initiated whenever the radius of the star approaches the Roche value. To avoid potential instabilities associated with a step function (e.g., oscillations of the radius around the Roche value), mass loss is actually allowed to begin a little short of R_R and given a very stiff radial dependence:

$$\dot{M} = \dot{M}_{\rm bin}(R/R_R)^{50}\,, \qquad (3)$$

for $R < R_R$, the Roche radius, and equals $\dot{M}_{\rm bin}$ for larger radii. Here $\dot{M}_{\rm bin}$ is arbitrarily equal to 0.001 $M_\odot$ yr^{-1} during helium burning and 0.01 $M_\odot$ yr^{-1} thereafter. Though our code has provision for nonconservative transfer, specifically nonzero α and β parameters as defined by Podsiadlowski et al. (1992), the calculations performed here were conservative, i.e., $\alpha = \beta = 1$.

For additional stability during the mass-losing phases of the evolution, a surface boundary pressure of from 200 to 500 dyn cm^{-2} was carried in all calculations. Attempts to calculate models with zero boundary pressure led to large oscillations of the radius caused, in the code at least, by an opacity instability. That Roche lobe overflow in these stars may be accompanied by Cepheid oscillations is an interesting, and so far as we are aware, unstudied possibility. For this work we attempted to suppress this instability.

A typical stellar evolution calculation to neon depletion took about 50,000 time steps and carried 500–700 zones.

2.3. *Specific Models*

For illustration, we first consider the evolution of a 15 $M_\odot$ star in a binary system with a 10 $M_\odot$ star initially separated by a distance of 3 AU (model 15A). For the semiconvective prescription employed ($F = 0.1$; Woosley & Weaver 1988; moderate semiconvection), the star's life is unaffected by the presence of a companion until helium burning is nearly complete. Halfway through helium burning ($Y_c = 0.50$) for example, the radius of the star is only 3.0×10^{12} cm, one-sixth of the Roche value, 1.22 AU. When the central helium abundance had declined to 0.050 by mass fraction, however, 155,000 yr before the star is due to explode, the stellar radius becomes equal to the Roche radius and rapid transfer begins. Prior to this time the star had lost only 0.2 $M_\odot$ to radiative mass loss. The luminosity at this point was 2.64×10^{38} ergs s^{-1} and the effective temperature 6150 K. The Roche radius was 1.82×10^{13} cm and the stellar radius 1.61×10^{13} cm (see eq. [3]).

Once begun, the mass transfer ensued very rapidly, essentially instantaneously so far as nuclear evolution of the core is concerned, slowing only after most of the envelope had crossed over. The radius throughout this epoch was allowed to become larger than the Roche radius, though it never became much more. An interesting effect kept the transfer from becoming dynamic. In order for mass to migrate, it must be lifted to the Roche radius. Since most of the matter initially resides near the base of the envelope, considerable energy must be expended overcoming the gravitational potential. For example, raising cold matter from a radius of 2×10^{11} cm (6 $M_\odot$ in the 15 $M_\odot$ model; about 1.5 $M_\odot$ above the helium core) to a large radius requires 4×10^{15} ergs. Considerably less energy is actually required since the internal energy is comparable to the gravitational potential, but a mass-loss rate of 0.001 $M_\odot$ yr^{-1} still requires on the order of 10^{38} ergs s^{-1}, comparable to the luminosity of the star. As a consequence the envelope transfer takes place on a Kelvin-Helmholtz timescale for the primary, very roughly 10,000 yr. If one attempts a larger mass-loss rate, the luminosity declines, and the radius shrinks. A smaller mass-loss rate allows the luminosity to inflate the star to a larger radius. The mass transfer is thus self-limiting (eq. [3]).

We illustrate our calculation with some specific points. When the original 15 $M_\odot$ star had decreased to 6.70 $M_\odot$, its envelope mass was 2.45 $M_\odot$. This took 16,000 yr. The surface luminosity at this point was 2.27×10^{38} ergs s^{-1}, but there was an appreciable gradient in L between the hydrogen shell and the surface. The maximum L in this region was 2.39×10^{38} ergs s^{-1}, the difference reflecting the work required to raise material at the base of the envelope to a large radius for transfer. The radius of the star at this point was 2.07×10^{13} cm and the Roche radius 1.99×10^{13} cm and increasing. Mass transfer was continuing, but at a slower rate. The central helium abundance had actually increased somewhat at this point ($Y_c = 0.062$) owing to the growth of the helium convective core.

Fifty thousand years later, when the total mass was 6.18 $M_\odot$, this first major mass transfer episode ended as the radius of the primary shrank (just) inside its Roche value. The envelope mass here was 2.1 $M_\odot$, the luminosity 2.41×10^{38} ergs s^{-1} with no appreciable gradient throughout the envelope. The stellar radius was 1.96×10^{13} cm and the Roche radius 2.15×10^{13} cm. Mass transfer was continuing at a greatly reduced rate, now on a nuclear timescale—5×10^{-6} $M_\odot$ yr^{-1}.

By central helium depletion ($Y_c = 5 \times 10^{-4}$; another 50,000 yr later) the mass of the star had declined to 5.44 $M_\odot$; the hydrogen envelope mass was 1.10 $M_\odot$; and its composition 45% H, 53% He, 1.0% N, and 0.35% O, by mass. There were no gradients in the envelope composition. The luminosity, now provided by a combination of residual helium core burning, helium shell burning, and hydrogen shell burning, had increased to 2.58×10^{38} ergs s^{-1}, only slightly below the maximum luminosity near the base of the envelope, 2.66×10^{38} ergs s^{-1}, and the mass loss had increased to 5×10^{-5} $M_\odot$ yr^{-1}. The radius was 2.36×10^{13} cm and the Roche radius 2.46×10^{13} cm. The central composition of the carbon-oxygen core was 18.4% C, 79.2% O, 2.1% Ne, and traces of other elements. It was then 120,000 yr since the mass transfer had begun.

Just prior to carbon ignition, 23,000 yr later, when the central temperature was 5.0×10^8 K, the envelope mass had declined further to 0.44 $M_\odot$ (stellar mass 4.78 $M_\odot$), implying a nearly constant mass-loss rate in this interval near 3×10^{-5} $M_\odot$ yr^{-1}. At this point, however, the star was making a rapid transition from a hydrogen shell power source to a helium shell source and its structure was changing rapidly. The luminosity

at this point had risen to 2.84×10^{38} ergs s^{-1} and the radius, 2.73×10^{13} cm, close to Roche value, 2.84×10^{13} cm. Consequently the instantaneous mass transfer rate was again $6 \times 10^{-5}\ M_\odot\ yr^{-1}$.

Finally, about 10,000 yr later, when the star was well into neon burning and the envelope had reached its final configuration, the total mass of the star was 4.53 $M_\odot$ and the envelope mass (external to the point where $X_H = 0.01$) was 0.19 $M_\odot$. Mass transfer was still occurring at $2 \times 10^{-5}\ M_\odot\ yr^{-1}$. The radius was 2.82×10^{38} ergs s^{-1} compared to a Roche radius of 3.04×10^{13} cm. The luminosity was 3.29×10^{38} ergs s^{-1}, and the star virtually indistinguishable, save for its surface composition and deformation, from a 15 $M_\odot$ star that had lost no mass (Table 1). The composition of the surface (and of the wind) was 44% He, 54% H, 1.0% N, 0.3% Ne, and various trace elements. The carbon abundance in the envelope was very low, 0.012% by mass, down by about 100 compared to nitrogen as a result of CN-processing. Since the star was filling its Roche lobe at the time it exploded, we expect that the hydrogen envelope was quite deformed. The radius of the helium core is very small, 5×10^{10} cm, and would not be very distorted. This helium core additionally contains 95% of the mass. For a star with a centrally condensed mass distribution and a mass much less than the secondary, the ratio of the axes approaches 3:2 (Szebelehely 1967). Here 4.53/21.47 = 21% is close enough to zero that the ratio should be close to that value (Lin 1993).

The critical properties of the hydrogen envelope are not expected to appreciably change after neon depletion. Typically, the life expectancy of the star has become less than 1 yr at this point. Considerable computational expense was saved then by "pasting" the envelope and outer helium core structure of the star evolved without mass loss onto the inner helium and heavy-element core of a previously evolved presupernova model (Weaver & Woosley 1994). The density, radius, and compositional structure were usually smooth at the juncture point though the mating process often entailed a readjustment of $\sim 0.05\ M_\odot$ in the total mass of the star. This adjustment occurred in the helium shell and had no effect on the hydrogen envelope structure.

One exception to this general rule (that the outer layers evolve negligibly after neon ignition) was the class of 11 $M_\odot$ models. These stars are very close to degeneracy in their cores and the structure of both the helium core and envelope can still change appreciably even during oxygen burning, especially for the small mass envelopes considered here. The transposition of the envelope in both models 11A and 11B resulted in an artificial mass loss from the helium core of 0.1 $M_\odot$ and a discontinuity of a factor of 2 in the density at the juncture point (base of the hydrogen envelope). Because 11 $M_\odot$ models are probably too faint as presupernova stars to satisfy observational constraints on SN 1993J and because the shock washed out even a factor of 2 jump in the density without appreciable consequence, we did not spend extra time examining the late time structural changes that affect these special models.

Other 15 $M_\odot$ models had similar histories though the numbers differ because of the chosen initial orbital separations. Models 15A, 15B, and 15C converged on very similar final hydrogen envelope masses near 0.20 $M_\odot$. This apparently is the minimum value required for a massive star with a helium-rich ($Y \approx 0.50$) envelope to maintain a radius of 2–3 AU as a presupernova. Since a smaller radius truncates mass loss and radiative mass loss may be inconsequential during the brief remainder of the star's life, it would not be surprising to find a number of supernova progenitors with similar envelope properties. It is interesting that our light curve and photometric studies in later sections will independently demonstrate that this is the sort of envelope that is required to produce SN 1993J.

Model 15D ended with a substantially more massive envelope. In fact, it had a larger mass at all stages of its evolution and entered the critical transition between helium and carbon burning with a mass (at $T_c = 5 \times 10^8$ K) of 6.20 $M_\odot$ (compared with 4.78 $M_\odot$ for model 15A; see above). Mass loss continued at a self-limiting value of $2 \times 10^{-5}\ M_\odot\ yr^{-1}$ through carbon ignition and burning, giving the final properties summarized in Table 2 and and Figures 2 and 3. The Roche radius of model 15D is smaller because of its larger mass and this makes its presupernova radius somewhat smaller than, for example, model 15C. Model 15D does not resemble SN 1993J. We shall find that its light curve is, if anything, closer to that of a Type II-L supernova. It is clear that larger radii and masses could be obtained by increasing the initial orbit separation beyond 5 AU (or considering nonconservative aspects of the transfer process). Given the deformed and possibly pulsating nature of the envelopes of these stars, the radii and luminosities given in Table 2 must be regarded as approximate.

We shall also find that model 13B *is* a good representation of SN 1993J, so it is worth discussing its evolution in some detail. Qualitatively, it resembled model 15A (and 15B and 15C) described above. Roughly half-way through helium burning

TABLE 2

BINARY EVOLUTION

Model[a]	Initial a (AU)	Final a (AU)	Companion ($M_\odot$)	Final R_R (AU)	Mass ($M_\odot$)	M_{env} ($M_\odot$)	$R_{pre\ SN}$ (10^{13} cm)	$L_{pre\ SN}$ (10^{38} ergs s^{-1})
11A	2	6.4	8	1.60	3.09	0.20	2.17	1.66
11B	3	8.2	8	2.11	3.43	0.54	2.57	1.67
13A	3	9.1	9	2.29	3.67	0.15	2.86	2.32
13B	4	12.0	9	3.03	3.69	0.18	3.86	2.33
13C	4.5	13.4	9	3.38	3.71	0.20	4.33	2.32
13D	5	14.3	9	3.65	3.80	0.28	4.89	2.32
15A	3	7.8	10	2.03	4.54	0.19	2.80	3.32
15B	4	10.5	10	2.71	4.55	0.19	3.56	3.39
15C	4.5	11.6	10	3.02	4.57	0.21	4.03	3.38
15D	5	9.8	10	2.70	5.51	1.16	3.48	3.31
15E	3	8.1	10	2.08	4.45	0.37	2.76	2.12

[a] Model name gives mass the star originally had on the main sequence.

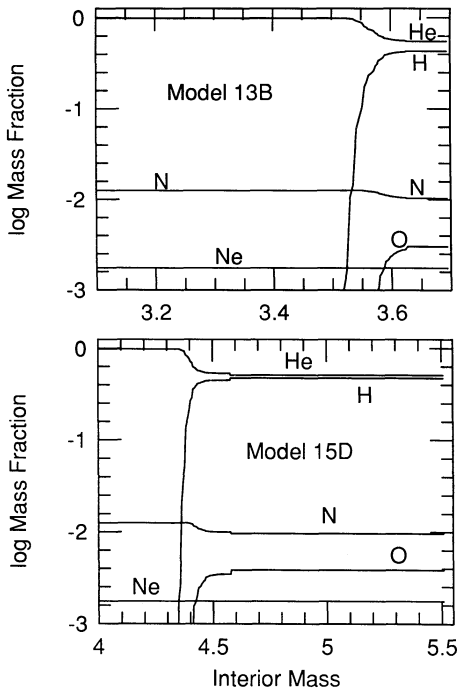

FIG. 2.—Final composition in the outer regions of models 13B and 15D. The primordial iron abundance is near 10^{-3} by mass fraction in both stars. All other elements, including carbon, are less abundant than 0.001 by mass fraction. Model 13B is a good progenitor for SN 1993J; model 15D has too large an envelope and a light curve that peaks too late.

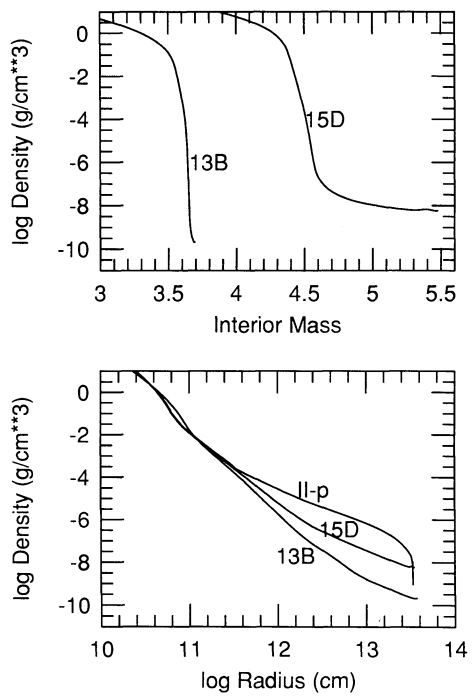

FIG. 3.—Density as a function of mass and radius in the outer regions of models 13B and 15D. Model 15D has an extensive convective envelope of near constant density ($\sim 10^{-8}$ g cm^{-3}). Model 13B has only a small surface convective zone. Also shown in the lower panel is the radial distribution of density in a typical Type IIp progenitor, a 15 $M_\odot$ red supergiant that has not experienced mass loss (Weaver & Woosley 1994).

($Y_c = 0.63$; stellar age = 15 million yr), the star was still a blue supergiant ($L = 1.50 \times 10^{38}$ ergs s^{-1}; $R = 3.17 \times 10^{12}$ cm). Less than 0.1 $M_\odot$ of the star's original envelope had been lost at that point by radiative processes. Mass transfer began somewhat earlier than in model 15A when the central helium mass fraction was 0.16. The luminosity of the star at this point was 1.61×10^{38} ergs s^{-1}, the radius, 1.56×10^{13} cm, and the Roche radius, 1.77×10^{13} cm. Thirty thousand years later the mass of the star had declined to 5.28 $M_\odot$ and the envelope mass to 1.93 $M_\odot$. Rapid mass transfer was still in progress with $R = 2.79 \times 10^{13}$ cm, $L = 1.29 \times 10^{38}$ ergs s^{-1}, $R_R = 2.99 \times 10^{13}$ cm, and $\dot{M} = 3 \times 10^{-4}$ $M_\odot$ s^{-1}. The central helium abundance was unchanged.

At central helium depletion ($Y_c = 10^{-4}$), 300,000 yr later, the stellar mass was 4.36 $M_\odot$ and the mass-loss rate 3×10^{-5} $M_\odot$ yr^{-1}. Forty thousand years later the central temperature reached 5×10^8 K and the mass of the star was 3.91 $M_\odot$, the envelope mass was 0.39 $M_\odot$, the radius, 3.72×10^{13} cm, the Roche radius 4.2×10^{13}, the luminosity 1.99×10^{38} ergs s^{-1}, and the mass transfer rate 2×10^{-5} $M_\odot$ yr^{-1}. During neon burning, 16,000 yr later, the star's mass was 3.69 $M_\odot$ with other properties as given in Table 2 and Figures 2 and 3.

Model 15E, a 15 $M_\odot$ star with reduced semiconvection, had a qualitatively different sort of evolution, one important difference being that mass transfer started at the beginning of helium burning rather than at the end. It is well known that stars evolved using the LeDoux criterion burn helium as red supergiants (e.g., Lauterborn, Refsdal, & Weigert 1971). This star first moved to the red in the Hertzsprung-Russell diagram and began mass transfer when the helium mass fraction was 0.98. The luminosity at that point was 1.40×10^{38} ergs s^{-1} and the radius, 1.78×10^{13} cm. Rapid mass transfer ensued. Before the helium abundance had declined to 0.97, the mass of the star had been reduced to 4.95 $M_\odot$ and the stellar radius moved back inside the Roche lobe. However, unlike the model with regular semiconvection, the helium core was not sharply defined. Hydrogen persisted at the 1% level even at 3.01 $M_\odot$. Between 3 and 4.3 $M_\odot$ there was a gradient in the hydrogen to helium concentration. The luminosity at this point had climbed to 2.12×10^{38} ergs s^{-1}. Continuing evolution proceeded on a helium burning timescale. By the time the central helium mass fraction reached 0.50, 380,000 yr later, radiative mass loss had reduced the mass of the star further to 4.67 $M_\odot$. By helium depletion, 600,000 more years later, the mass had still only declined to 4.62 $M_\odot$ but the star was once again expanding, but still considerably less than the Roche radius. As the star made the transition to carbon ignition and a surface luminosity supplied by helium shell burning, it again filled its Roche lobe and began to transfer mass. The star died with a mass of 4.49 $M_\odot$ and other properties as shown in Table 2 and Figures 4 and 5. The mass transfer rate at death was $\sim 10^{-5}$ $M_\odot$ yr^{-1}.

3. EXPLOSION AND MIXING

Explosion in all models was simulated using a piston placed near the outer edge of the iron core. Specifically the piston was placed at the location where, moving inward, the electron mole number Y_e exhibited a discontinuous jump (due to convection and electron capture in silicon shell burning) to substantially less than 0.50. In the 11 and 13 $M_\odot$ models this was the same as the location where the iron mass fraction dropped below 0.5, and for the 15 $M_\odot$ models it was a little interior to that point (Table 3).

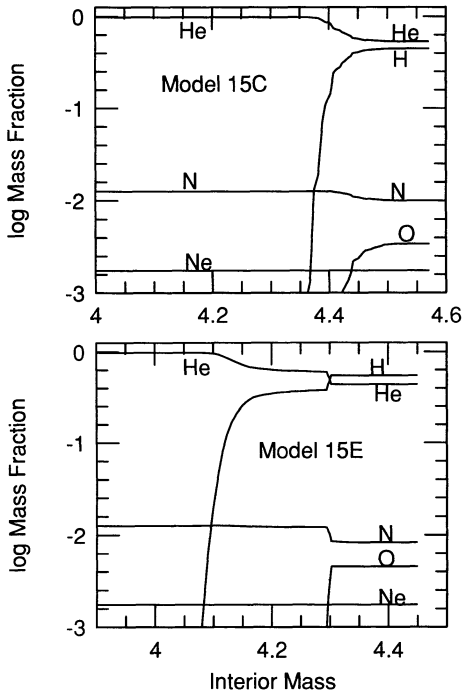

FIG. 4.—Composition in the outer regions of two 15 $M_\odot$ presupernova stars (models 15C and 15E) which had identical binary, parameters and mass loss parameterization. However, model 15E had a semiconvective diffusion coefficient 1000 times less than model 15C (see text).

In each case, the piston was first moved *inward* smoothly over a period of 0.45 s from a starting radius of 1327 km (11 $M_\odot$), 1543 km (13 $M_\odot$), or 1161 km (15 $M_\odot$) to a radius of 500 km. Overlying material in the inner few tenths $M_\odot$ in the presupernova star followed the piston in. The piston was then moved rapidly outward at a velocity of 29,000 km s^{-1} (11 $M_\odot$), 19,400 km s^{-1} (13 $M_\odot$), or 18,800 km s^{-1} (15 $M_\odot$) and gradually slowed as if on a ballistic trajectory appropriate to the interior mass and radius (Woosley & Weaver 1982). The piston was halted and held stationary, however, when a radius of 10,000 km was reached. This happened after 2.75 s (11 $M_\odot$), 3.95 s (13 $M_\odot$), or 3.55 s (15 $M_\odot$). These parameters, especially

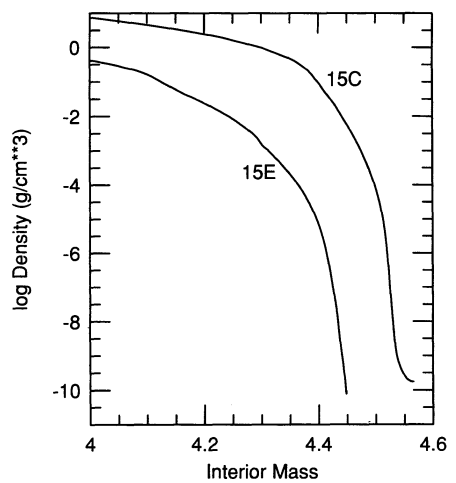

FIG. 5.—Density distribution in the outer layers of models 15C and 15E (see Fig. 4).

TABLE 3

PROPERTIES OF SUPERNOVA MODELS

Model[a]	Fe Core[b] ($M_\odot$)	Piston Mass[c] ($M_\odot$)	Mass Cut ($M_\odot$)	KE_∞ (10^{51} ergs)	M(^{56}Ni) ($M_\odot$)
11.....	1.32	1.32	1.32	1.29	0.093
13.....	1.41	1.41	1.46	1.31	0.151
15.....	1.32	1.29	1.43	1.22	0.121

[a] All models of the same initial mass (e.g., 13A, 13B, and 13C) had the same core structure and explosion parameterization.

[b] The iron core was nominally defined as that point in the pressupernova model where the mass fraction for all species heavier than $A = 50$ exceeded 0.50.

[c] The piston mass was that location where the piston was placed—in each star the place where Y_e made an abrupt change from 0.50 to ~0.47.

the initial piston velocity outward, were adjusted so as to give a nearly constant kinetic energy at infinity in all of the models, ≈ 1.2–1.3×10^{51} ergs.

Motion of the piston set up a shock wave which traversed the supernova. In the inner regions the shock was sufficiently strong to give rise to explosive nucleosynthesis which was followed in detail. Nucleosynthesis of 200 isotopes was followed in all zones (Weaver & Woosley 1994), but will not be discussed here. Instead we are interested in the abundances of just those few (abundant) elements, especially ^{56}Ni, that affect the light curve and spectrum. Not all of the material external to the piston was ejected in all the models (Table 3). As the shock moved through regions of increasing ρr^3 in the mantle, it slowed. Since the sound speed was still high, this information was propagated as pressure waves back into the innermost material, some of which slowed below the escape speed and fell back (Herant & Woosley 1993). Most of this material which fell back was composed of ^{56}Ni and helium. Clearly the mass of ^{56}Ni that is ejected will depend on details of the explosion mechanism that were not well modelled here. The amount actually ejected in our calculation is given in Table 3. In the most successful light curve calculations to be described later, this amount was artificially adjusted (by removing inner zones) to be 0.073 $M_\odot$ in all the models.

As the shock encountered the base of the hydrogen envelope, where ρr^3 also increases dramatically, it slowed again. At this point we anticipate that a multidimensional calculation would show mixing. Such calculations are planned in the near future, but have not yet been carried out. It is clear however that, owing to the low mass of the envelope, mixing will be far less extensive than in Type IIp supernovae (Herant & Woosley 1994) or in SN 1987A. Still the slowing of the shock does produce a mild "reverse shock" (Fig. 6) which leads to extra heating and a shell of high-density material in the ejecta which persists even after the expansion has become homologous (Fig. 7). This reverse shock should also lead to mixing in the outer helium core. We simulated this mixing in an artificial fashion, in part because the smoothness of the light curve suggests that compositional stratification was not preserved in the explosion. The final composition in both the mixed and unmixed versions of model 13B are given in Figures 8 and 9. Some mixing was presumed to occur in the inner core, even though the reverse shock never got there. This is assumed to be a consequence of the explosion mechanism itself and of the slowing of the shock in the core of heavy elements.

The final velocity, (mixed) composition, and (one-dimensional) density structure are given for several other models in Figures 10–14.

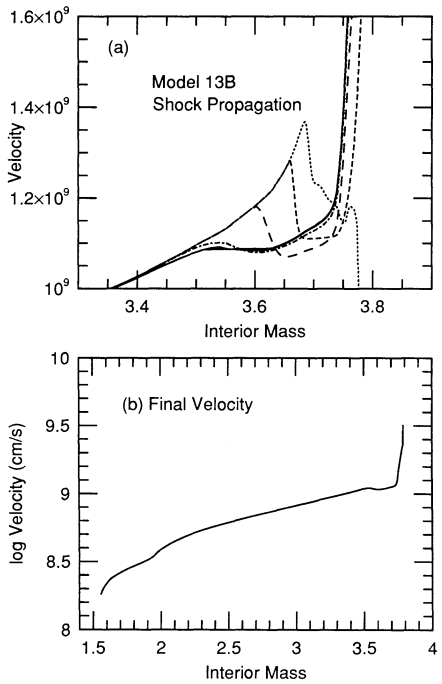

FIG. 6.—Velocity evolution in model 13B. Fig. 6*a* shows the velocity in the outer layers at 2.0×10^4 s (near shock break out; *dotted line*), 3.0×10^4 s (*short dash*), 5×10^4 s (*long dash*), 1×10^5 s (*dot-short dash*), 2×10^5 s (*solid*), and 3×10^7 s. The latter two curves are indistinguishable. All times are measured since core collapse. Fig. 6*b* gives the terminal velocity profile. 0.016 $M_\odot$ of ejecta (seven zones) are moving faster than 20,000 km s^{-1}.

4. LIGHT CURVE CALCULATION

4.1. *Computational Method*

The light curves for the models in Table 2 were calculated twice. One calculation employed the KEPLER stellar evolution and hydrodynamics code (Weaver et al. 1978) and assumed an opacity given strictly by electron scattering (Ensman & Woosley 1988) and radiative transport corresponding to a flux-limited diffusion of blackbody radiation. The light curves obtained for several 13 and 15 $M_\odot$ models are given in Figure 15. The second calculation, a multigroup radiation transport calculation, employed a more physical description of the atomic physics, opacity, and gamma-ray deposition and warrants some discussion. The computer code employed

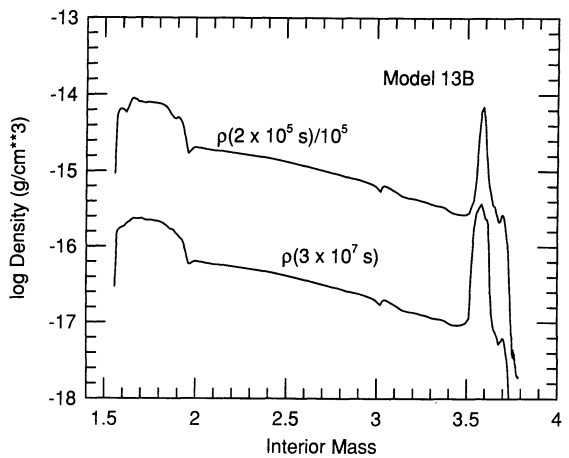

FIG. 7.—Density distribution in model 13B at two different times. The actual density at 2×10^5 s has been divided by 10^5 for display. Note the homologous scaling, $\rho \propto t^{-3}$ obeyed after 2×10^5 s and the dense shell at 3.6 $M_\odot$ (corresponding to the flat portion of the velocity profile in Fig. 6). The high density is a consequence of the deceleration of the shock in the helium-hydrogen interface (Fig. 6). In a multidimensional calculation the high-density material might be in the form of clumps.

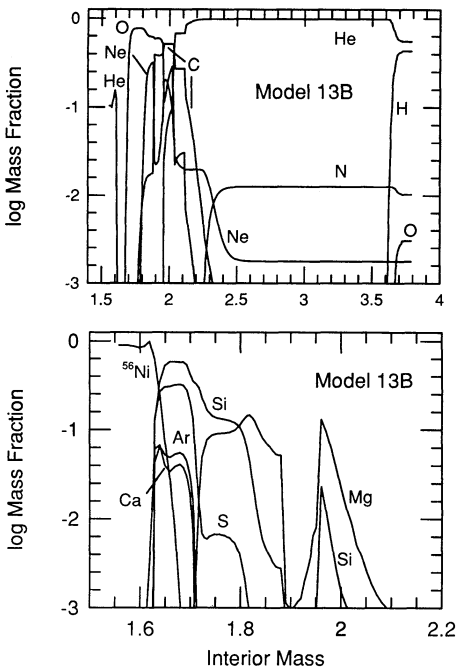

FIG. 8.—Final composition in model 13B following explosive nucleosynthesis but without any mixing.

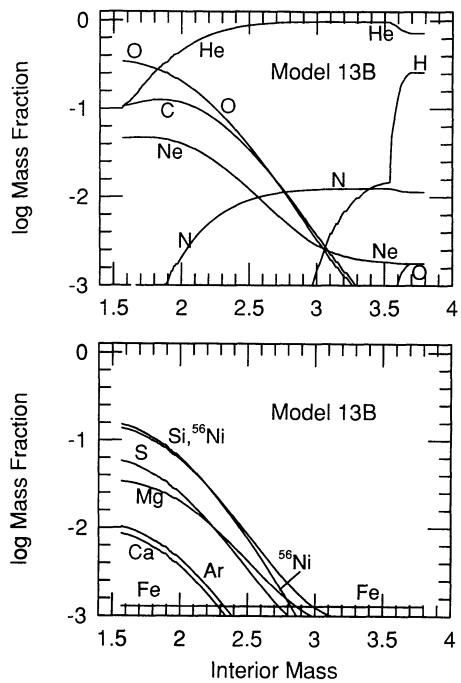

FIG. 9.—Final composition in model 13B following a moderate amount of (artificial) mixing. This is the composition employed in the light curve and spectral calculations. The total ^{56}Ni mass is 0.073 $M_\odot$ and the hydrogen mass fraction is 0.01 at 9800 km s^{-1}. This mixing is typical of that employed in all "mixed" models.

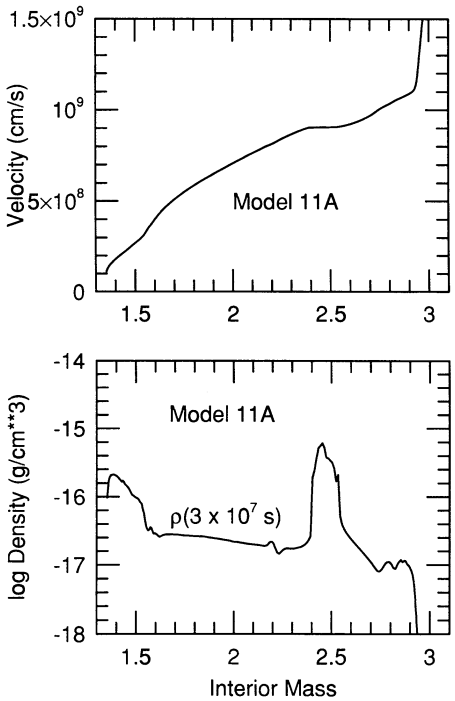

FIG. 10.—Final velocity for model 11A evaluated when the supernova is 3×10^7 s old (*top*) and the density structure at the time (*bottom*).

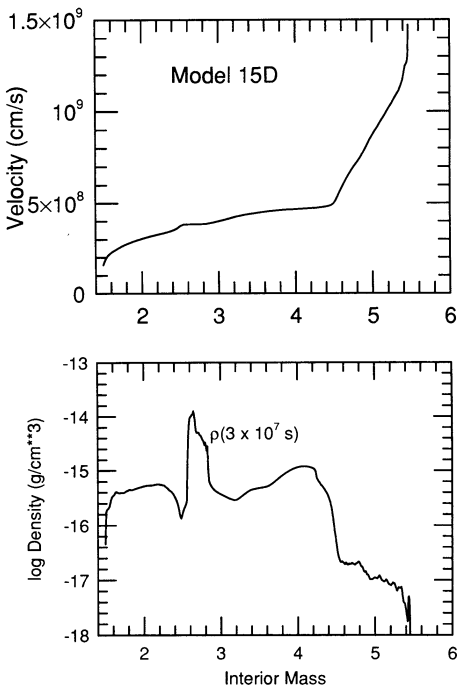

FIG. 12.—Final velocity for model 15D evaluated when the supernova is 3×10^7 s old (*top*) and the density structure at that time (*bottom*). Note the quite different density structure from Figs. 7, 10, and 11 owing to the more massive hydrogen envelope and the deeper penetration of the reverse shock.

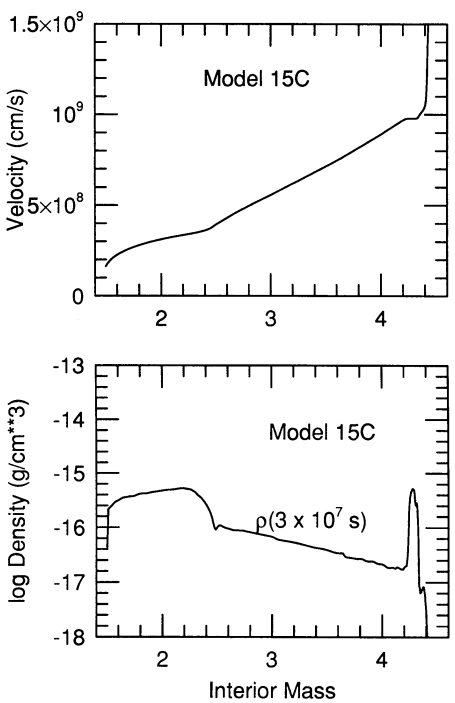

FIG. 11.—Final velocity for model 15C evaluated when the supernova is 3×10^7 s old (*top*) and the density structure at that time (*bottom*).

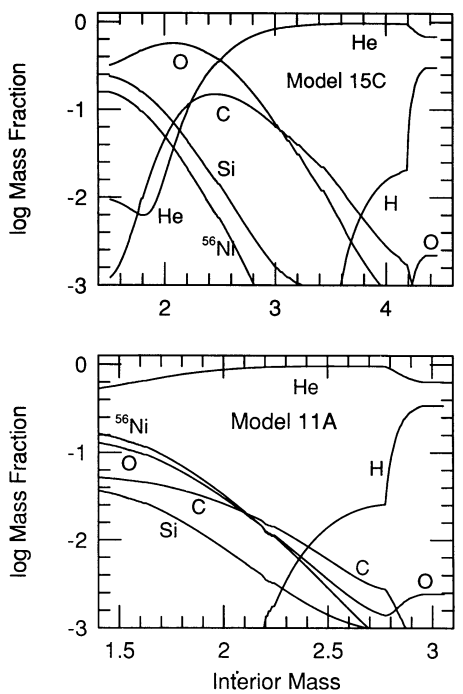

FIG. 13.—Final composition of models 15C and 11A following a moderate amount of (artificial) mixing. These were the compositions employed in the light curve calculations. The ^{56}Ni mass has been adjusted to 0.73 $M_\odot$ in both models. The 15 $M_\odot$ model obviously makes more ^{16}O and other heavy elements.

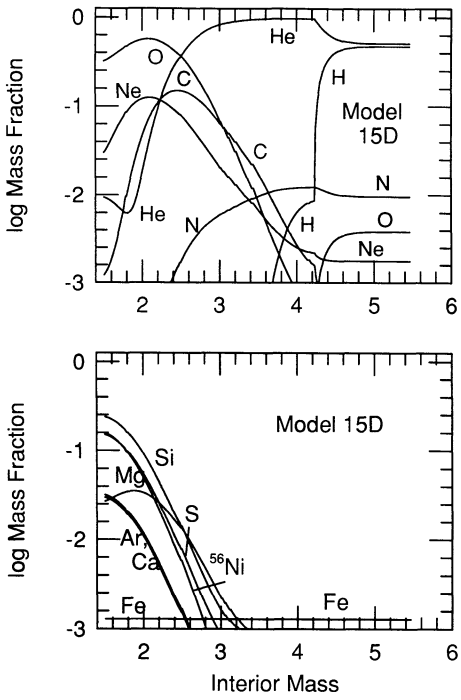

FIG. 14.—Final composition for model 15D following a moderate amount of (artificial mixing).

was a modified version of the EDDINGTON program described by Eastman & Pinto (1993). The chief modification, made in order to obtain a result in a reasonable time, was to replace the non–LTE gas equation of state in the EDDINGTON code by the much simpler Saha-Boltzmann equation. Simplifying the gas equation of state in this way allows computational efforts to be concentrated on details of the radiation field distribution.

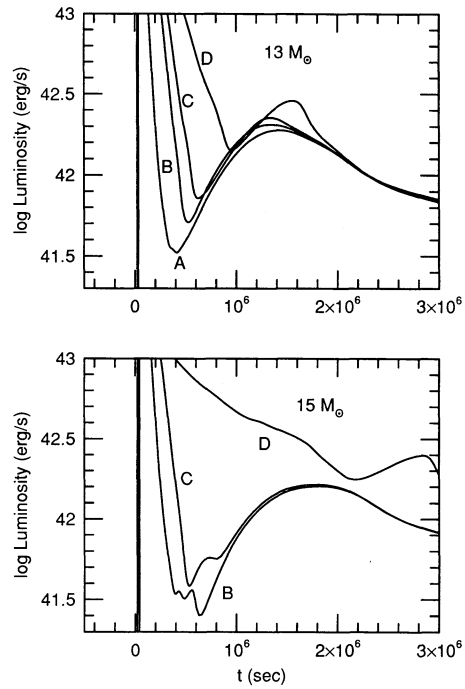

FIG. 15.—Light curves of the 13 and 15 $M_\odot$ models calculated using KEPLER and an opacity due solely to electron scattering. The assumed ^{56}Ni mass in all models was 0.073 $M_\odot$ and the assumed *gamma*-ray opacity at late times, 0.054 cm^2 g^{-1}.

At each time step in the EDDINGTON code, the time-dependent radiation transport equation was solved in the co-moving frame on a fixed frequency grid of 500 bins ranging in energy from 200 μm to 30 Å, and a Lagrangian mass grid of 80 shells. Following solution of the transport equation, a temperature correction was applied using an approximate lambda operator procedure to split the radiation field into local and nonlocal components as described in Eastman & Pinto (1993). The program cycles between temperature correction and solution of a new radiation field until the temperature and level population corrections are less than 1%.

The opacity included Thomson scattering from free electrons, free-free, and bound-free photoionization from ground and excited states of H I, He I and II, C I to VI, O I to VIII, Si I to X, S I to X, Ca I to XII, Fe I to XIV, Co I to XIV, and Ni I to XIV. The opacity also included an equally important contribution from approximately 2000,000 lines of the most abundant ions. The majority of the transition probabilities for this was taken from a much larger compilation by Kurucz (1991) and was approximated as an "expansion opacity" as described by Eastman & Pinto (1993).

One major restriction of this code is that it does not calculate accelerations and thus can only be applied to a homologously coasting configuration in which the density structure has "frozen out." In practice that meant that the models were usually evolved to age 1–2 × 10^5 s in the KEPLER code and then mapped into the EDDINGTON code. Any remaining nonmonotonicity in the velocity profile (due, for example, to the presence of a reverse shock, Fig. 6) was "smoothed out" by setting velocities in the core equal to their radius divided by the elapsed time. We do not expect this approximation to have any effect on the recombination epoch (first few days) of the supernova. Eventually a multidimensional calculation will be necessary to correctly depict the "clumpy" density structure and late time evolution of the supernova (McCray 1993; Li, McCray, & Sunyaev 1993).

Energy deposition from γ-rays produced in the decay chain $^{56}\mathrm{Ni} \rightarrow {}^{56}\mathrm{Co} \rightarrow {}^{56}\mathrm{Fe}$ was computed by performing a radiation transport solution for each γ-ray line produced in the decay. The emissivity for this calculation was given by the local volume rate of γ-ray production, and the opacity was determined as follows: the ratio of scattered to incident energy of a γ-ray which scatters at an angle θ in a zero temperature electron gas is given by

$$\frac{E'}{E} = \frac{1}{1 + (E/m_e c^2)(1 - \cos\theta)} . \tag{4}$$

We assume that all photons scatter at an angle $\theta_{\rm scat}$, and in the present set of calculations have taken $\theta_{\rm scat} = 90°$, so that a scattering photon gives up a fraction $(1 + E/m_e c^2)^{-1}$ of its energy. The scattering part of the opacity is taken as

$$\sigma_{\rm scat} = \frac{N_e \sigma_{\rm KN}(E_0)}{1 + (E_0/m_e c^2)(1 - \cos\theta_{\rm scat})} , \tag{5}$$

and the absorptive part as

$$k_{\rm abs} = N_e \sigma_{\rm KN}(E_0)\left[1 - \frac{1}{1 + (E_0/m_e c^2)(1 - \cos\theta_{\rm scat})}\right] , \tag{6}$$

where E_0 is the initial photon energy, N_e is the total (bound

and free) electron density, and $\sigma_{KN}(E_0)$ is the Klein-Nishina cross section. In essence, this approach assumes that the photon energy stays the same, but that the number of photons decreases through scattering. In actuality, of course, photons themselves are not destroyed by scattering. It is their energy which is diminished. However, this simple approximation works well. Taking $\theta_{scat} = 90°$ gives results which agree with more detailed Monte Carlo calculations, although better agreement could probably be had by using a smaller value of θ_{scat}, consistent with the shape of the differential scattering cross section (see, e.g., Jackson 1975). For example, at 115 days in model 13B, detailed Monte Carlo calculations predict the fraction of decay energy which escapes to be 0.53, whereas the present scheme gives the fraction as 0.47.

The formal solution to the comoving frame transport equations gives, among other quantities, the emergent spectrum in the lab frame. Although the EDDINGTON calculations are a more detailed treatment of the radiation field than typically performed in supernova light curve studies (500 frequency bins vs. 1), the frequency resolution is still somewhat low, and the velocity structure of P Cygni spectral features is not well resolved. However, exploratory calculations utilizing 4 times as many frequency grid points have been found to give nearly identical results for the bolometric light curve and only minor differences in the broad-band light curves.

From the emergent spectrum we can calculate broad-band photometric colors for comparison with observations. The analytic filter functions used for this are described in Eastman & Kirshner (1989). The accuracy of the computed emergent spectrum and of the synthetic photometry is variable. It should be accurate early on, when the density at the photosphere is high and the atmosphere is hot. However, as the atmosphere expands and thins out, departures from LTE at the surface become more and more significant. Beginning around the time of the second peak in SN 1993J and especially 2 weeks later, broad bands such as B and V are more and more dominated by emission lines. Ultimately, the remnant becomes an optically thin nebula excited by nonthermal Compton electrons. As has been known since the 1930s (e.g., Menzel 1962), excitation conditions in nebulae are far from thermal equilibrium. We should not be surprised, therefore, if the agreement between synthetic colors and observations grows progressively worse with time. The computed bolometric luminosity should still be quite accurate during the phase, since it is determined mainly by the rate of energy deposition from radioactive decay, and the opacity treatment is accurate at large optical depth where the gas is closer to being in thermodynamic equilibrium.

4.2. *Stages in the Bolometric Light Curve*

The light curve has several stages, each of which is sensitive to a specific set of physics and how it is modeled.

First comes shock break out (Fig. 16). Model 15C is typical. The shock erupts from the surface (T_{eff} first rises to 10^4 K) 1.99×10^4 s after core collapse. The luminosity continues to rise rapidly to a maximum of 3.3×10^{44} ergs s^{-1} at 2.78×10^4 s. The FWHM of this luminosity peak is 8000 s. Similarly the effective temperature rises to 125,000 K. At 2×10^5 s post collapse, when the link between KEPLER and EDDINGTON was made, the luminosity had fallen to 1.7×10^{43} ergs s^{-1} and T_{eff} was 20,000 K. The good agreement of the KEPLER and EDDINGTON light curves at these early times suggests that the KEPLER curves (Fig. 16) are a good representation of shock break out and the first few days of evolution. The calculation suffers, of course, from employing a single temperature for both the radiation and matter and thus is probably an underestimate of both the luminosity and effective temperature at these early times (e.g., Ensman & Burrows 1992).

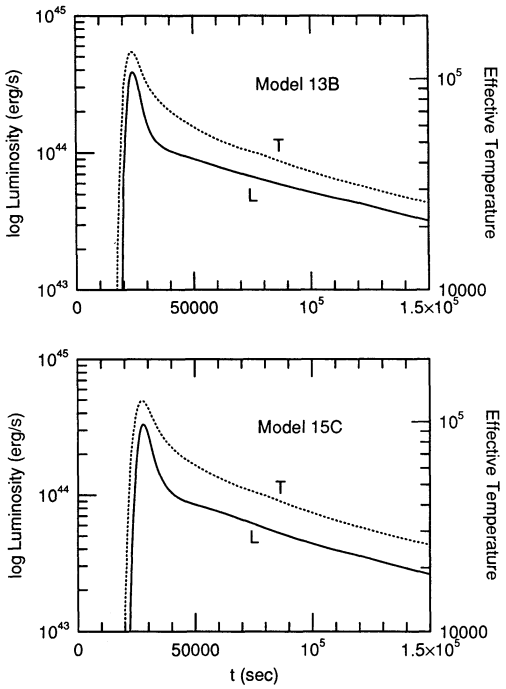

FIG. 16.—Bolometric light curves and effective temperature for models 13B and 15C calculated during the first 1.5×10^5 s following core collapse using KEPLER. The actual values for both T and L near shock break out are probably underestimated by ~50% owing to the coarse zoning. Note a shock propagation time from the collapsed iron core to the surface near 2.0×10^4 s for both models.

Next comes an epoch of envelope expansion and recombination, both of hydrogen and of helium which, had the mass of the envelope been large, would have corresponded to the plateau of a Type IIp supernova. Instead, because of the low mass, low density (much lower than in a Type IIp; Fig. 3), high velocity, and the rise in the helium abundance as the photosphere moves in, the light curve falls very rapidly. Because of these same factors, but especially because of the high helium abundance, the effective temperature is higher than on the plateau of a Type IIp, ~7000 K versus 5500 K. In order for the light curve to fall to its observed value at the minimum 6 days after the explosion, we find that the envelope mass must have been very small. In particular, a 1 $M_\odot$ envelope is far too large (see Fig. 1, Woosley 1991, and Fig. 15, model 15D), even for a light curve calculated using only electron scattering opacity. Such a large mass would also overly tamp the expansion of the other 1.5–3 $M_\odot$ of ejecta so that the second peak was delayed. This requirement of a low mass is consistent with what is expected for the binary transfer described in § 2.

The remainder of the light curve is radioactive in origin. The beginning of the rise to second peak happens, as in SN 1987A, when the outward moving diffusion wave of energy deposited by ^{56}Ni and ^{56}Co decay meets with the inwardly moving recombination front. The timing and slope of this rise are sensitive to the opacity, explosion energy, mass of the ejecta and, in obvious ways, to the mass of the ^{56}Ni produced explosively and the degree to which the core has been mixed. One does not expect as much mixing in this supernova as in SN 1987A

because of the lower mass envelope and the diminished importance of the reverse shock. However, there is likely to be some (poorly determined) amount of mixing of the core brought about by the explosion mechanism itself (Herant & Benz 1992; Herant, Benz, & Colgate 1992). It will be interesting to study, observationally, the consequences of this mixing in an object that had a weak reverse shock. So far as the light curve is concerned, more mixing leads to an earlier rise to the second peak and thus a less pronounced minimum. The light curve also begins to decline a little earlier and, of course the X-ray and γ-ray line signals are stronger and commence earlier.

The time and luminosity of the second peak also depend on the same parameters and it is difficult to obtain a unique solution because there can be some trade-off among the various factors. A smaller mass of ^{56}Ni, for example, leads to a light curve that not only is fainter but peaks earlier (Woosley 1991). But a smaller mass of ejecta, larger kinetic energy, or lower opacity could have similar effects.

The decline after the second peak continues to be sensitive to all the factors above and to others that may not be modeled well in the present calculation. One factor, which is minor in the present context is the hydrodynamic effect of the ^{56}Ni decay. This is included, in a crude one-dimensional way, in the KEPLER calculation, but there the opacity is not realistic. It is not included in the EDDINGTON calculation which assumes homology. For most models the star was evolved with KEPLER out to $1–2 \times 10^5$ s after core collapse, and then mapped into the EDDINGTON code. We have performed a test calculation in which the velocity field at the time of the link was modified to have the asymptotic velocity (determined by evolving the star with KEPLER to 3×10^7 s). The light curve for both cases are nearly identical to each other, indicating that for these models hydrodynamic evolution which takes place after the time of the link has negligible effect on the light curves computed with EDDINGTON.

More important and much more difficult to model is the effect of clumping. The degree of clumping is unknown, but based on the level of density contrast seen in two-dimensional models of Type IIp supernovae (Herant & Woosley 1994), a factor of 3 might not be unusual at this epoch. McCray (1993) and Li et al. (1993), for example, have presented spectroscopic evidence that the core of SN 1987A may be quite clumpy. Such density fluctuations can dramatically reduce the diffusion time (consider, for example, the contrasting diffusion times of a homogeneous sphere of mass M, and a collection of equivalent mass comprised of a large number of more compact spheres bounded by the same radius. The ratio of the diffusion times would go approximately as the ratio of clump density to mean density). Perhaps this is why there has been such difficulty in the past in getting light curves for Type Ib supernova to decline as rapidly as the observations demand (Ensman & Woosley 1988; Woosley, Langer, & Weaver 1993).

For present purposes, what this means is that we cannot definitively rule out a model just because it peaks a little late or declines too slowly after peak. For this reason we have not tried to "tune" our models in order to achieve *exact* agreement with the observations.

4.3. *Numerical Results for the Bolometric Light Curve*

The resulting bolometric light curves from the detailed radiation transport calculation (EDDINGTON) are presented for model 11A–B, 13A–D, and 15B–C in Figures 17–19, along with bolometric data for 93J from Schmidt et al. (1993), assuming

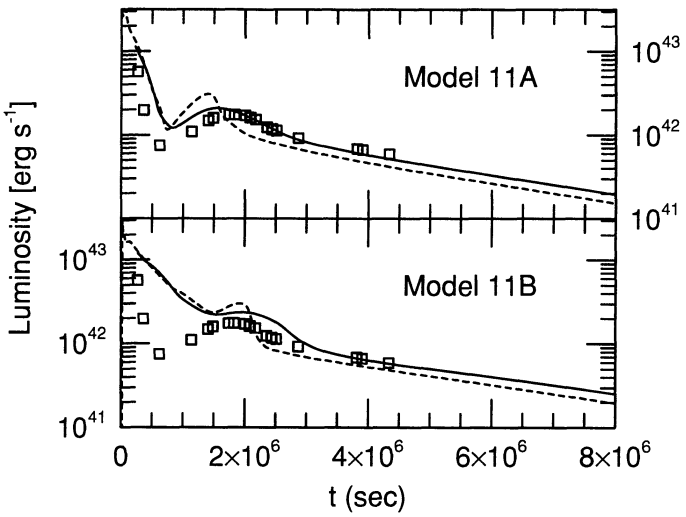

FIG. 17.—Comparison of EDDINGTON (*solid line*) and KEPLER (*dashed line*) light curves for the first 90 days of models 11A and 11B with bolometric data for SN 1993J (Schmidt et al. 1993).

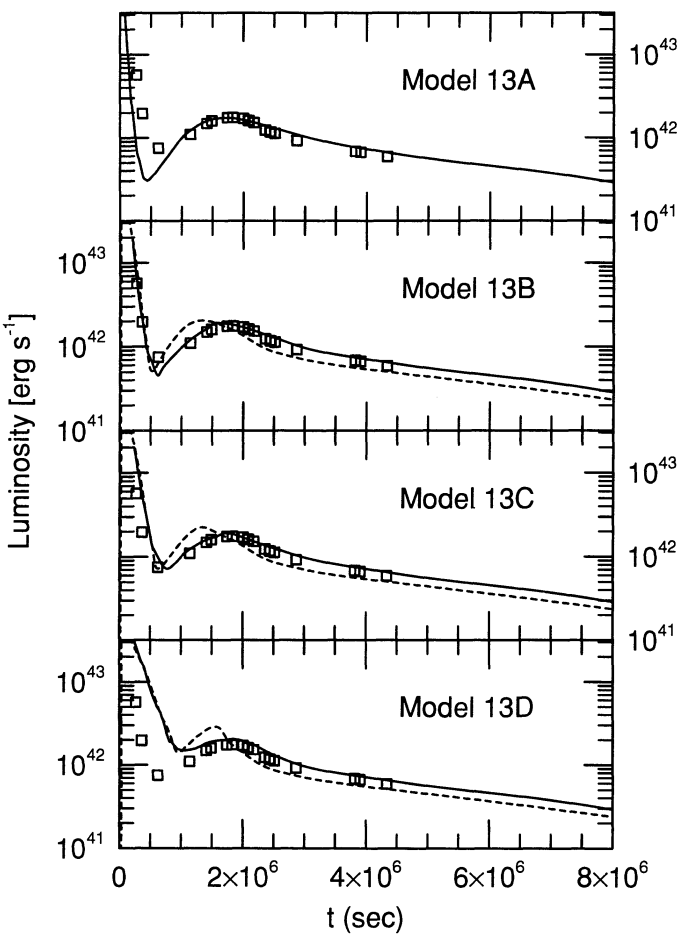

FIG. 18.—Comparison of EDDINGTON (*solid line*) and KEPLER (*dashed line*) light curves for the first 90 days of models 13A, 13B, 13C, and 13D, with bolometric data for SN 1993J.

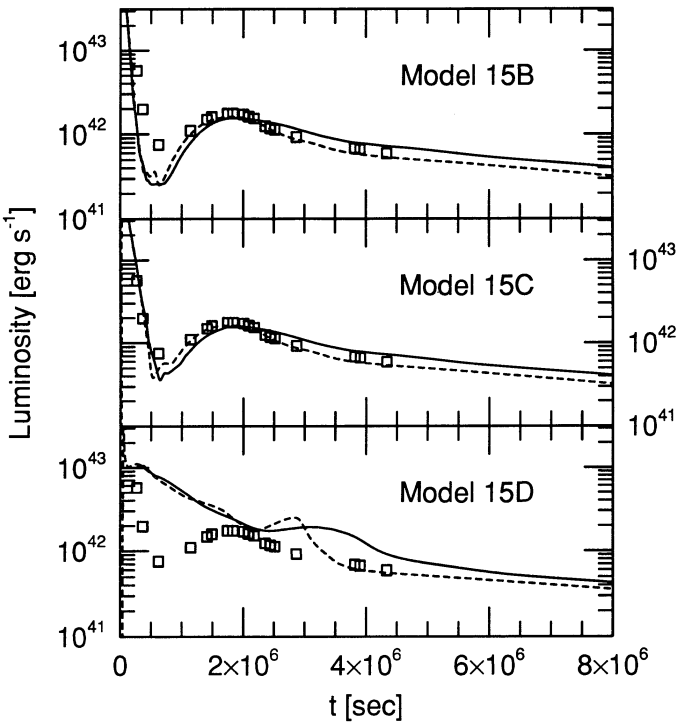

FIG. 19.—Comparison of EDDINGTON (*solid line*) and KEPLER (*dashed line*) light curves for the first 90 days of models 15B, 15C, and 15D with bolometric data for SN 1993J.

the explosion occurred on 1993 March 27.5. The additional opacity of the detailed calculation leads to a delay in the minimum as well as a broader light curve that peaks later. On the tail of the light curve, the EDDINGTON code gives a more accurate estimate of the gamma-ray deposition which it treats as a nonlocal process (KEPLER assumes a local deposition given by the total column depth to the surface).

In terms of the bolometric light curves alone, and with due consideration for both the errors in the models and the possible uncertainty in the distance to M81, models 11A, 13B, 13C, and 15C all do a fine job. This points up a certain degeneracy in the solutions. Without invoking presupernova observations, as were so valuable with SN 1987A, the bolometric light curve alone does not give us the progenitor mass. However, it cannot have been less than 11 $M_\odot$ and still have made adequate ^{56}Ni, and the presupernova observations probably do not allow anything much over 16 $M_\odot$ (or the equivalent helium core thereof; Aldering et al. 1993).

The sensitivity of the bolometric light curve to the mass of ^{56}Ni produced in the explosion is illustrated in Figure 20, where bolometric light curves of model 13B, with 0.05, 0.073 (the standard value), and 0.09 $M_\odot$ of ^{56}Ni, are plotted against the data of Schmidt et al. (1994), who assumed a distance to M81 of 3.3 Mpc. By the time of the second peak, the brightness is nearly proportional to the mass of ^{56}Ni, but the luminosity still exceeds the instantaneous rate of energy input from radioactive decay (§ 6). The best fit is obtained for a ^{56}Ni mass around 0.07 $M_\odot$ with an acceptable range of 0.01 $M_\odot$ around that value. If the more recent distance measurement of Freedman et al. (1994) is adopted, 3.63 $\pm$ 0.34 Mpc, then nickel mass rises to almost 0.09 $M_\odot$. These values are similar to the $\sim$0.07 $M_\odot$ found for SN 1987A (Suntzeff & Bouchet 1990; Suntzeff et al. 1991) and the $\sim$0.07 $M_\odot$ found for the Type IIp SN 1990E

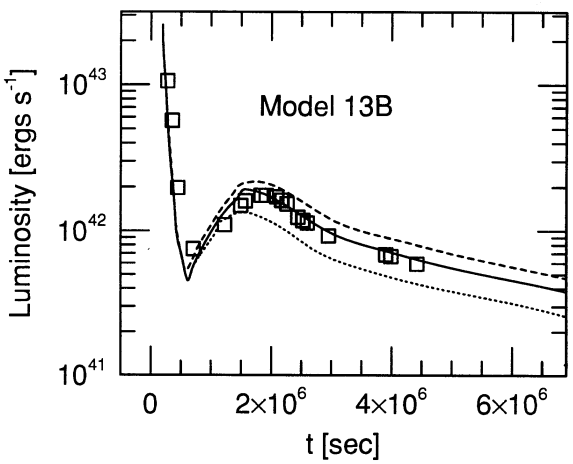

FIG. 20.—Comparison of the EDDINGTON light curves during the first 70 days of model 13B for a ^{56}Ni mass equal to 0.05, 0.073 (the standard value), and 0.09 $M_\odot$. Also shown are the bolometric data of Schmidt et al. (1993).

(Schmidt et al. 1994). The ^{56}Ni mass estimate here is sensitive to uncertain assumptions regarding the distance and reddening to SN 1993J, but it is interesting that SN 1987A may have produced slightly *less* of this isotope than SN 1993J. The progenitor star for SN 1987A was almost certainly larger than SN 1993J (20 $M_\odot$ vs. 15 $M_\odot$), which would suggest that the ^{56}Ni mass is not a monotonically increasing function of supernova mass. This would not be surprising since the ^{56}Ni mass ejected is quite sensitive to details of both the convective history of the presupernova star and the explosion mechanism. Overall, though, one is struck more by the similarity of these three numbers than their small differences.

5. COMPARISON TO BROAD-BAND PHOTOMETRY

In the previous section we described how the EDDINGTON code calculates the bolometric light curve by first computing the LTE spectrum at each time step and then integrating this over all wavelengths. One can also compute the broad-band photometry by integrating the spectra over the various passbands. This is a very different calculation than just assuming (or deriving) a color temperature and using that to compute the various magnitudes for a blackbody (which the spectrum is not!). Figures 21, 22, and 23 compare B and V light curves for the models 11A, B, 13A, C, and D, and 15B, C, and D, with La Palma and Royal Greenwich Observatory observations of SN 1993J from Meikle et al. (1993) and Leuschner Observatory observations by Richmond et al. (1993), assuming a distance of 3.3 Mpc (Freedman & Madore 1988) and an extinction of $E(B-V) = 0.15$ (Schmidt et al. 1993; Wheeler et al. 1993). Figure 24 shows B and V photometry for model 13B and additionally U, Cousins R and I, all taken from Meikle et al. (1993) and Richmond et al. (1993), and the Johnson infrared J, H, and K bands (IAU Circ. 5741–5844). It is satisfying that the two models which most closely agree bolometrically with SN 1993J, namely model 13B and 13C, also do well in B and V, particularly during the early stages prior to the second peak. However, even in the best-fitting model 13C, breakdown of the LTE assumption becomes especially evident beyond the second peak. Subsequent to the second peak, B and V decay more slowly than the observations, and at the expense of the ultraviolet, which decays too rapidly. After about 70 days, emission shifts to wavelengths longward of V, and B and V fall too rapidly.

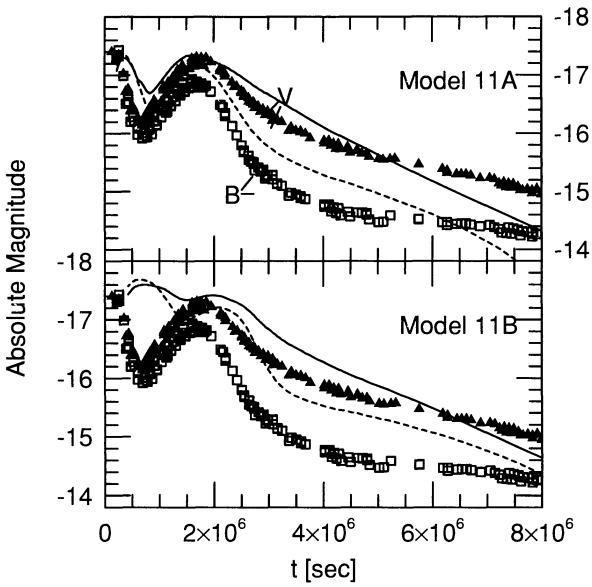

FIG. 21.—Comparison of B and V light curves for the first 90 days of models 11A and 11B with observations of SN 1993J (see text).

In Figure 24 it can be seen that after ~ 50 days, the rate of decline of B and V in model 13B is faster than in SN 1993J, while the model value of I decays too slowly in comparison to SN 1993J. The reason is that an increasing amount of the total luminosity comes out as Ca II infrared triple emission, $\lambda 8498$, $\lambda 8542$, and $\lambda 8662$. While this line is always strong in nebular

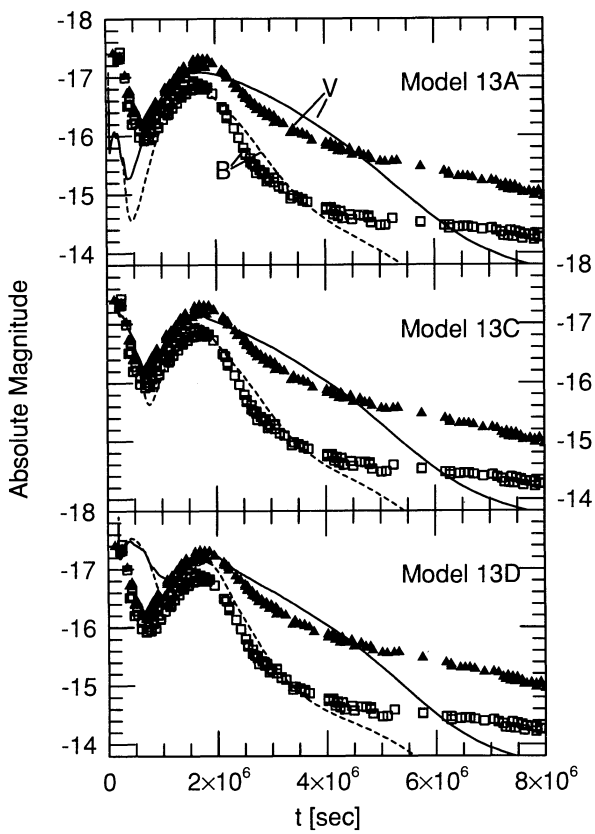

FIG. 22.—Comparison of B and V light curves for the first 90 days of models 13A, 13C, and 13D, with observations of SN 1993J.

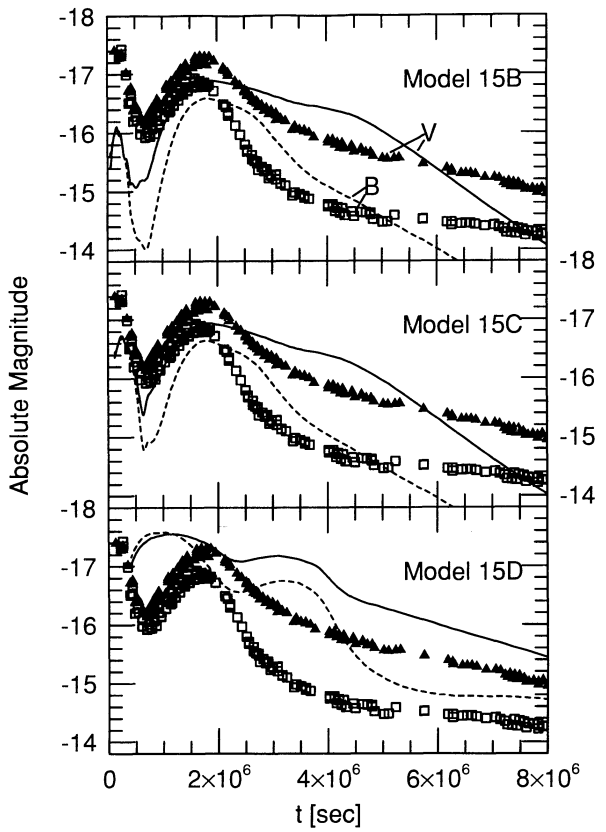

FIG. 23.—Comparison of B and V light curves for the first 90 days of models 15B, 15C, and 15D with observations SN 1993J.

phase Type II supernovae, its particular prominence here is entirely an artifact of assuming LTE. A more detailed non–LTE treatment would predict significantly more flux at shorter wavelengths, including emission in O I $\lambda 6300$, and forbidden Ca II $\lambda 7291$, $\lambda 7324$.

A similar problem exists with the U band. It can be seen in Figure 24 that at the first minimum, about 9 days after explosion, and afterward, the model U-band flux is much too small in comparison to observations. Similar behavior, in varying amounts, was found for all the models described here. Again, this is attributable to the LTE equation of state. It is well known from previous work on non–LTE models of photospheric phase supernovae that non-LTE scattering dominated photospheres have both a higher color temperature and excitation conditions than their LTE counterpart for equal effective temperature. For example, on 1993 April 12, SN 1993J had $U = -16.65$, $B = -16.56$, and $V = -16.88$, assuming the distance and reddening discussed above. For model 13B the LTE light curve code gives $U = -15.60$, $B = -16.50$, and $V = -16.87$ and is over magnitude too faint in U. Non–LTE atmosphere calculations with EDDINGTON (Eastman & Pinto 1993), for the same density structure and luminosity, given $U = -16.13$, $B = -16.56$, and $V = -16.89$. The more accurate non–LTE model spectrum is much brighter in U, although still a half a magnitude too faint in comparison to SN 1993J.

The non–LTE spectral evolution of SN 1993J will be discussed in another paper (Eastman & Pinto 1994).

We find that the models which give the best agreement with SN 1993J observations are those for which the composition

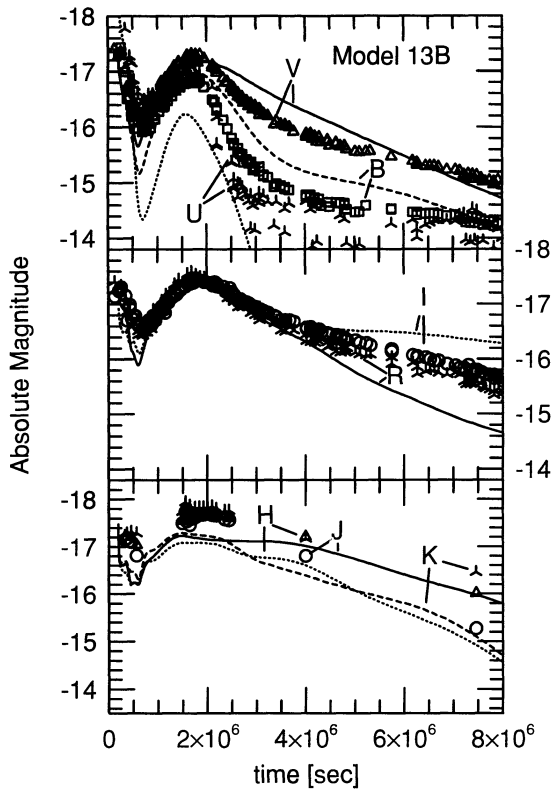

FIG. 24.—Johnson *U*, *B*, *V*, *J*, *H*, and *K* and Cousins *R* and *I* photometry for model 13B, and observations of SN 1993J (see text).

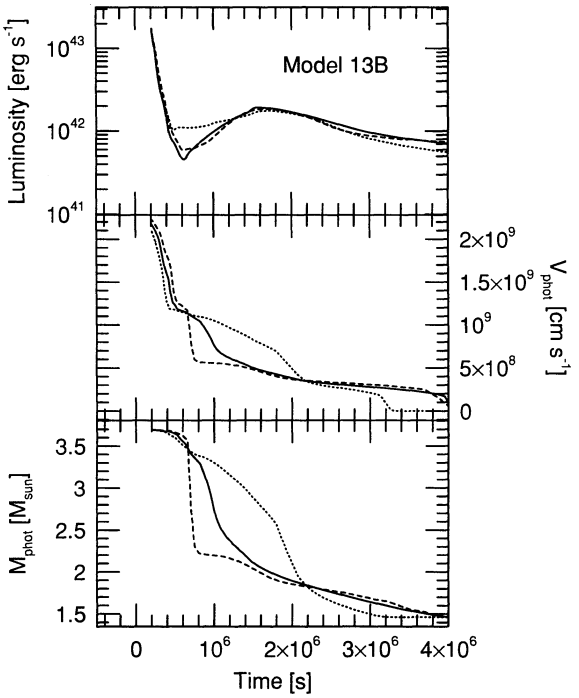

FIG. 25.—Comparative evolution of three versions of model 13B with various amounts of mixing, and ^{56}Ni mass equal to 0.073 $M_\odot$. The top, middle, and bottom panels display bolometric luminosity, photospheric velocity, and mass interior to the photosphere, respectively, for no mixing (Fig. 8–*dashed line*), mild mixing (Fig. 9–*solid line*), and a large amount of mixing (Fig. 26–*dotted line*).

has been mixed by a modest amount. Especially important is that some of the ^{56}Ni is mixed outward. Evidence for this is shown in Figure 25, which gives (*a*) light curves, (*b*) photospheric velocities, and (*c*) photospheric mass coordinates for the unmixed model 13B (Fig. 8), the moderately mixed model (Fig. 9), and an extreme case of a very mixed model (Fig. 26). In the very mixed model, which has ^{56}Ni mixed all the way to the surface, the first minimum is very shallow, γ-ray escape takes place earlier, and thus is slightly fainter out on the tail. Clearly, this model has been overly mixed. Bolometrically, there appears to be very little difference between the unmixed and moderately mixed models, and they are essentially identical out on the radioactive tail. However, they evolve very differently. The first minimum occurs at 10^6 s as the photosphere reaches down to the region of the H–He interface, which is at $v = 10^9$ km s^{-1}, or $M = 3.5\ M_\odot$. Although the optical color temperature is 8–9 $\times$ 10^3 K, the effective temperature is very close to 6 $\times$ 10^3 K in both the moderately mixed and unmixed models, a value which is well below recombination temperature of He I. When the photosphere reaches the H–He interface, the composition changes abruptly and, in the unmixed model, recombination proceeds rapidly. One day later it has receded all the way through the helium to the O–He interface, which is moving at 5 $\times$ 10^3 km s^{-1}. This is much too slow in comparison to SN 1993J, is far too blue on account of its photospheric, radius, and is spectroscopically very dissimilar.

A moderate amount of mixing of ^{56}Ni through the Si layer to the O–He interface enables decay energy to diffuse into the helium sooner, raising the temperature there and showing the rate of photospheric recession. A possible mechanism for the

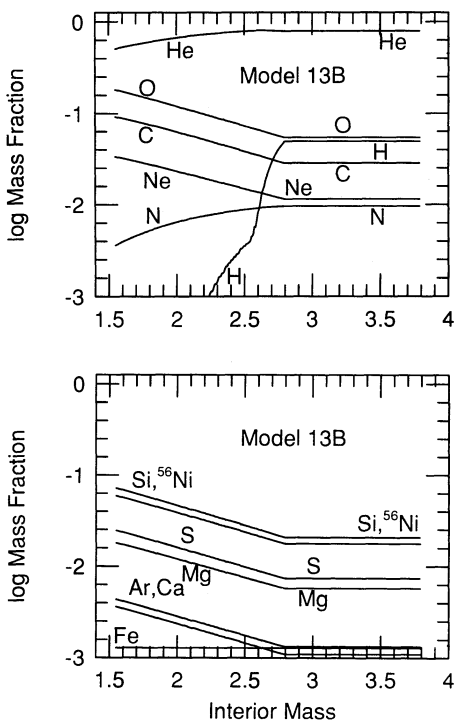

FIG. 26.—Final composition in model 13B following a very large amount of mixing. The mass fraction of ^{56}Ni at the surface is 0.018.

mixing might be Rayleigh-Taylor instability at the O–He interface. The conclusion that some mixing has taken place in SN 1993J seems unavoidable, although the question of exactly how much or how far out the ^{56}Ni must be mixed has not been precisely established. Swartz et al. (1993) conclude, based on non–LTE spectral synthesis calculations, that there has been no mixing in SN 1993J, but leave unanswered the question of how much mixing is "no mixing." It is likely that a modest amount of mixing can satisfy both the light curve and the spectroscopic constraints.

6. X-RAY AND GAMMA-RAY EMISSION

In order to provide an estimate of the expected gamma-ray line and Comptonized X-ray emission for SN 1993J we have computed the hard emission from two of our more realistic models—13B and 15C. Figure 27 shows the bolometric (ultraviolet through infrared) luminosity, $L_{\rm uvoir}$, instantaneous energy deposition rate from ^{56}Ni and ^{56}Co decay, $L_{\rm dep}$, and the sum of γ-ray line flux plus Compton X-ray continua, L_γ, for models 13B and 15C. One sees that, in both cases, $L_{\rm uvoir}$ exceeds $L_{\rm dep}$ at the second peak, but by $\sim$6 weeks after explosion they are very equal. The Compton X-ray and γ-ray luminosity peaks at around 10^7 s in model 13B, and a little later, at 1.4×10^7 s, in the more massive model 15C. In both models L_γ peaks at values near 10^{41} ergs s^{-1}.

By setting $\sigma_{\rm scat} = 0$ and the absorptive opacity $k_{\rm abs} = N_e \sigma_{\rm KN}(E_0)$, the γ-ray transport calculation described in § 4.1 can be used to compute the emergent luminosity of individual (unscattered) γ-ray line photons. The light curve for ^{56}Co 847 keV and 1238 keV decay photons is shown in Figure 28, both as total energy output, and as photon flux at 3.3 Mpc, for models 13B and 15C. The fluxes in these models (and the others) peak at about 120 days after the explosion, i.e., in 1993 August at $\sim 10^{-5}$ photons cm^{-2} s^{-1}. *This is not above the threshold of the Compton Gamma-Ray Observatory* (T. Gehrels, 1993, private communication). Preliminary data analysis from the OSSE team on *CGRO* (as reported in Chipman 1993) gave null results for line emission from SN 1993J during the intervals 9–15, 23–36, and 93–121 days after outburst. Preliminary results in the third interval give limits of $1.6 \pm 2.1 \times 10^{-5}$ and $0.7 \pm 1.9 \times 10^{-5}$ on the line emission at 847 and 1238 keV, respectively. To get the X-ray flux from Compton-scattered γ-rays, a full Monte Carlo calculation is necessary. This has also been done (as in Woosley, Pinto, & Hartmann 1989) with results given in Figure 29, again for a distance to M81 of 3.3 Mpc. At that distance, the continuum flux in the range 10–100 keV peaks at $\sim$30 days after explosion at values above 10^{-4}, X-ray emission lines of iron and other heavy elements are also prominent. The OSSE team (again, preliminary results cited in Chipman 1993) reported a marginal detection of hard X-ray continuum emission near 100 keV of $1.82 \pm 0.39 \times 10^{-3}$ photons cm^{-2} s^{-1} MeV^{-1} and $0.89 \pm 0.35 \times 10^{-3}$ photons cm^{-2} s^{-1} MeV^{-1}, respectively, during the intervals 9–15 and 23–36 days after explosion. The first value is far too bright to have been produced by radioactivity when the supernova was 1 week old (baring an unacceptably large amount of mixing). The second value is also large compared with our model predictions, but the preliminary nature of the OSSE values is to be emphasized, and it is hard to separate the supernova X-ray flux from other sources potentially in the same field of view, or the radioactive component from a component due to circumstellar interaction. The hard continuum was not seen by OSSE in the longer third interval.

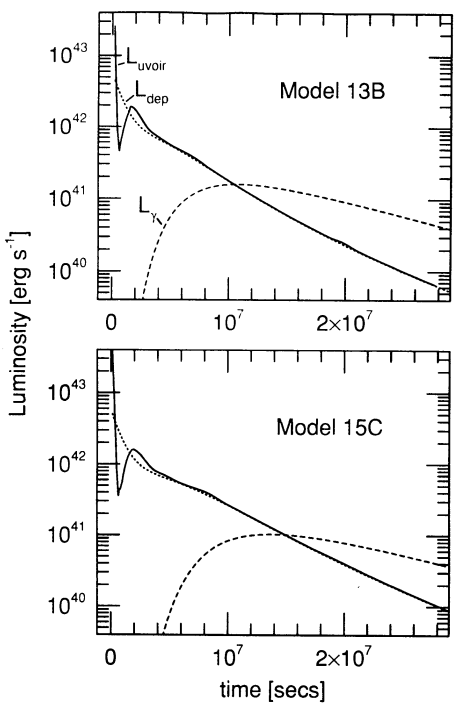

FIG. 27.—Various components of the bolometric light curve of (*top*) model 13B and (*bottom*) 15C. Note that the luminosity at second peak is larger than the instantaneous rate of radioactive power (the curve shown includes both ^{56}Ni and ^{56}Co decay).

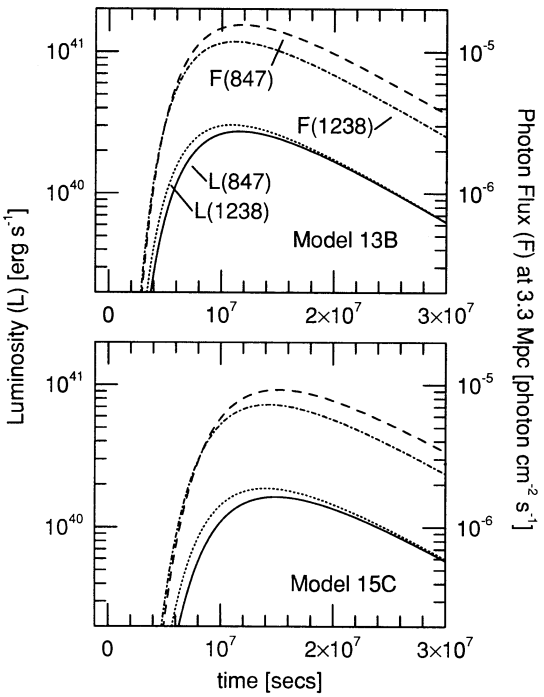

FIG. 28.—847 keV and 1238 keV light curves for model 13B and 15C. These models are typical of all those which give a credible fit to the optical light curve. The peak of gamma-ray line emission occurs in 1993 August, 120 days after the explosion and was not visible to *CGRO*. Photon fluxes, shown on the right axis, are normalized to a distance of 3.3 Mpc (Freedman & Madore 1988).

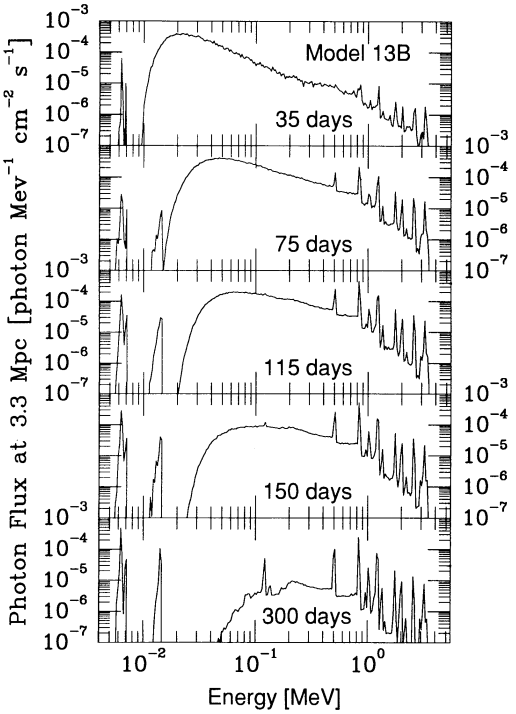

FIG. 29.—Comptonized X-rays for the same model shown in Fig. 28 at several times after the explosion.

Our calculated onset of X-ray continuum emission is very sensitive to the assumed mixing. The energy of a photon after n scatterings is approximately $m_e c^2/n$ (Xu 1989), and photons with energy $E_K \lesssim 20$ keV are destroyed by iron K-shell absorption. Therefore, X-rays emerge when the optical depth to ^{56}Co is $\tau_K \sim (m_e c^2/3E_K)^{1/2} \sim 3$. The time of X-ray emergence, t_X, therefore goes like $t_X \propto \tau_{56}^{1/2}$, and models which are more thoroughly mixed will brighten sooner.

Figure 30 compares the γ-ray light curves of model 13B with no mixing (Fig. 8), moderate mixing (Fig. 9), and much mixing (Fig. 26). Not surprisingly, the very well mixed model brightens much earlier than the other two cases. However, there is very little difference between the (more realistic) unmixed and moderately mixed models.

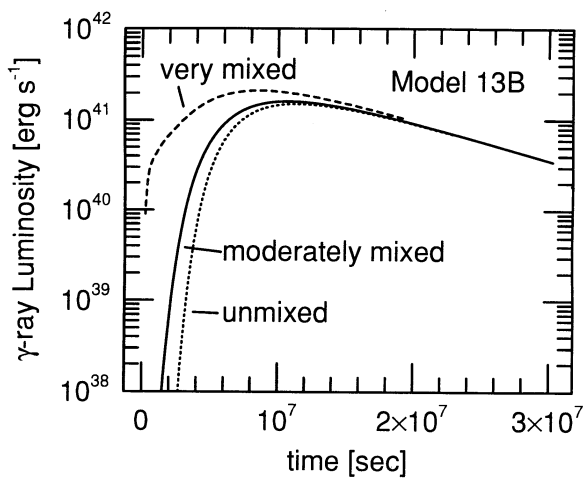

FIG. 30.—γ-ray light curves of model 13B with no mixing (Fig. 8), moderate mixing (Fig. 9), and much mixing (Fig. 26).

7. DISCUSSION AND CONCLUSIONS

In order not to violate restrictions on the luminosity of the progenitor and still produce the necessary amount of ^{56}Ni in the explosion, the progenitor of SN 1993J must have begun its life as a star of mass 13–16 $M_\odot$. In order to give a bolometric light curve that declined as rapidly as observations and exhibited a second peak no later than $\sim$20 days, the envelope mass at the time of explosion must have been small, certainly less than 0.5 $M_\odot$ and probably very near 0.2 $M_\odot$. Stars of this main-sequence mass are not expected to lose most of their envelope by radiative winds. It would also have been an incredible accident had 98% of the envelope been lost just as the star exploded. Thus we conclude that the star lost mass mainly because of exchange with a binary companion.

When one actually simulates the binary mass transfer, a pleasing coincidence emerges—for a variety of separations and companion masses, the final envelope mass converges on 0.2 $M_\odot$ (Table 2). This is apparently the minimum mass required to support a red supergiant photosphere at a radius of 2–3 AU for a composition of roughly half hydrogen and half helium. For a given binary separation at death, a larger mass of envelope would sustain a larger radius at the given luminosity and thus cause rapid mass transfer to continue that would reduce the envelope mass to 0.2 $M_\odot$. A radius of 2 to 3 AU is required in order to obtain good agreement with the light curve during the first week of the supernova. The term "stellar radius" may not be well-defined here, however, because (*a*) the supernova progenitor was highly deformed (with an axis ratio about 0.7 to 1) at the time of its explosion, because it continued to fill its Roche lobe; (*b*) the progenitor may have been a pulsating variable; and (*c*) at least in low-mass models (11 $M_\odot$), the envelope structure may have been changing even during the last few years of the star's life (during oxygen and helium shell burning).

The mass loss from the progenitor occurred in two stages, the first during the late stages of helium core burning ($Y_c \sim$ 0.05–0.10) when the star became a red supergiant. Most of the envelope was lost at this time during a dynamic phase that lasted $\sim$30,000 yr, the Kelvin-Helmholtz time for the envelope, and occurred about 100,000–200,000 yr prior to the explosion. A second stage of rapid mass transfer occurred as helium was depleted in the core and the surface luminosity of the star switched from a helium core plus hydrogen shell power source to helium shell burning. This caused a brightening of the star and additional mass transfer that continued right up until the time the star died. Typical mass transfer rates at the time of explosion were $\sim 10^{-6}$ to 10^{-5} $M_\odot$ yr^{-1}, though how much of this mass was actually being lost from the binary system is very uncertain. The wind inferred by X-ray and radio observations may indicate that this transfer was not completely conservative, or perhaps the companion star had a (radiative) wind as well. The possible pulsational instability of the presupernova star also implies that all mass-loss estimates near the time of the explosion are very approximate.

Because the primary star (i.e., the presupernova) lost approximately 10 $M_\odot$ of its mass roughly 100,000 yr ago during a very short interval, one might expect an extended torus of this mass around the supernova. Moving at 10 km s^{-1}, it would now have a radius of about a parsec.

We find that the bolometric light curve can be well fitted by a variety of models having helium cores in the range 2.8–4.5 $M_\odot$ and envelope masses near 0.2 $M_\odot$, consistent with that

expected for stars that satisfy the luminosity constraints on the progenitor. Somewhat larger masses might have been tolerable were the limits on presupernova luminosity to be relaxed, but beyond a helium core mass of 6 $M_\odot$ (main-sequence mass 20 $M_\odot$) it would take much more than the usual 10^{51} ergs of kinetic energy to obtain a narrow second peak for the light curve occurring as early as 20 days (Ensman & Woosley 1988). The successful models all have initial ^{56}Ni in the range 0.06–0.08 $M_\odot$ for a distance to M81 of 3.3 Mpc (Freedman & Madore 1988). The best value is near 0.07 $M_\odot$. Adopting the more recent estimate for the distance to M81 of Freedman et al. (1994), 3.63 ± 0.34 Mpc, increases this estimate to nearly 0.09 $M_\odot$, somewhat larger than in SN 1987A. Explosion energies near 1.2×10^{51} ergs give good agreement, though, lacking knowledge of the exact presupernova radius and mass, one cannot makes as precise a statement regrading the explosion energy as in SN 1987A.

Obtaining models that give as good agreement with the color photometry in U, B, and V bands has proved more difficult than fitting the bolometric light curve. Qualitatively good agreement can be obtained on the first peak, but the LTE–spectra at the second and beyond are increasingly dominated by emission features which are not well reproduced by an LTE equation of state. The U band light curve, in particular, is difficult to reproduce well in LTE. Better agreement is found when the assumption of LTE is dropped. Nonetheless, the LTE light curve code is a very useful tool for studying Type II supernovae as it gives approximate and qualitatively correct results in a reasonable amount of time. We show elsewhere that it also gives a very good representation, even of the photometry, for ordinary Type IIp supernovae on their plateaus.

The conversion of SN 1993J into a Type IIb supernova from what was originally expected to be Type IIp had important ramifications for its emission in the X-ray and γ-ray bands. The gamma-ray line emission from radioactive decay and the Comptonized X-rays accompanying those decays will be much brighter and peak at an earlier time than either a Type IIp or SN 1987A. Our models give a peak flux of 1×10^{-5} (3 Mpc/D)^2 photons cm^{-2} s^{-1} during August of 1993. This was not detectable by the *Compton Gamma-Ray Observatory*, but would have been seen by some other gamma-ray astronomy missions currently being discussed (i.e., INTEGRAL, Teegarden 1993). This same model also gives Comptonized X-ray emission which should also be sought should a future supernova of similar magnitude appear.

One very exciting prospect is that the binary companion to the supernova, a star which must have been larger than 15 $M_\odot$ and less than 25 $M_\odot$ when the supernova exploded, is still there—presently being baked inside the supernova. It should emerge when the supernova's luminosity has declined by a factor of 10^4, i.e., about 3 yr after explosion. In the model we have described, less than half the mass of the binary was ejected in the explosion. There may have been a large kick imparted by the explosion mechanism, and that would be very interesting to study, but baring that, the companion star is now bound in an eccentric orbit with the newly born neutron star. Someday, millions of years from now, when the companion becomes a red giant, we shall have a very strong X-ray source. X-ray source or not, it will be fascinating to see a star that has recently had 10 $M_\odot$ of hydrogen and helium dumped on it and then baked in a supernova. It will appear first in the ultraviolet, where it emits a larger fraction of its luminosity than does the supernova.

This work has been supported by the NASA Theory Program (NAGW-2525), the National Science Foundation (AST 91-15367) and, at Livermore, by the Department of Energy (W-7405-ENG-48).

REFERENCES

Aldering, G., Humphreys, R. M., & Richmond, M. 1993, AJ, submitted
Arnett, W. D., Bahcall, J. N., Kirshner, R. P., & Woosley, S. E. 1989, ARA&A, 27, 629
Baron, E., Hauschildt, P. H., Branch, D., Wagner, R. M., Austin, S. J., Filippenko, A. V., & Matheson, T. 1993, ApJ, 416, L21
Bartunov, O. S., Blinnikov, S. I., Pavlyuk, N. N., & Tsevtkov, D. Yu. 1994, A&A, 281, L53
Blakeslee, J., & Tonry, J. 1993, IAU, Circ., No. 5758
Chiosi, C., & Maeder, A. 1986, ARA&A, 24, 329
Chipman, E. 1993, *Compton Observatory* Sci. Rep. No. 132, Goddard Space Flight Center, 1993 August 12
de Jager, C., Nieuwenhuijzen, H., & van der Hucht, K. A. 1985, in IAU Symp. 116, Luminous Stars and Associations in Galaxies, ed. C. De Loore, A. Willis, & P. Laskarides (Dordrecht: Reidel), 109
Eastman, R. G., & Kirshner, R. P. 1989, ApJ, 347, 771
Eastman, R. G., & Pinto, P. A. 1993, ApJ, 731
———. 1994, in preparation
Eggleton, P. P. 1983, ApJ, 268, 368
Ensman, L. M., & Burrows, A. 1992, ApJ, 293, 742
Ensman, L. M., & Woosley, S. E. 1988, ApJ, 333, 754
Filippenko, A. V. 1988, AJ, 96, 1941
Filippenko, A., & Matheson, T. 1993, IAU Circ., No. 5787
Filippenko, A., Matheson, T., & Ho, L. C. 1993, ApJ, 415, L103
Frank, J., King, A., & Raine, D. 1992, Accretion Power in Astrophysics (2d ed.; Cambridge: Cambridge Univ. Press), chap. 4
Freedman, W. L., & Madore, B. F. 1988, ApJ, 332, L63
Freedman, W. L., et al. 1994, ApJ, submitted
Hashimoto, M., Iwamoto, K., & Nomoto, K. 1993, ApJ, 414, L105
Herant, M., & Benz, W. 1992, ApJ, 387, 294
Herant, M., Benz, W., & Colgate, S. A. 1992, ApJ, 395, 642
Herant, M., & Woosley, S. E. 1994, ApJ, 425, 814
Höflich, P., Langer, N., & Duschinger, M. 1993, A&A, submitted
Hsu, J. J., Ross, R. R., Podsiadlowski, Ph., & Joss, P. C. 1991, in ESO/EIPC Workshop on SN 1987A and Other Supernovae, ed. J. Danziger & K. Kjär (Garching: ESO), 37
Humphreys, R. M., Aldering, G. S., Bryja, C. O., & Thurmes, P. M. 1993, IAU Circ., No. 5739
Jackson, J. D. 1975, Classical Electrodynamics (2d ed.; New York: Wiley)
Kurucz, R. L. 1991, in Stellar Atmospheres: Beyond Classical Models, ed. L. Crivellari, I. Hubeny, & D. G. Hummer (Dordrecht: Kluwer), 441
Lauterborn, D., Refsdal, S., & Weigert, A. 1971, A&A, 10, 97
Li, H., McCray, R., & Sunyaev, R. A. 1993, ApJ, 419, 824
Lin, D. 1993, private communication
Magnier, E., Lewin, W., Lubin, L., van Paradijs, J., Zimmerman, U., & Fabbiano, G. 1993, IAU Circ., No. 5741
McCray, R. 1993, ARA&A, 31, 175
Meikle, P., et al. 1993, Gemini, 40, 1–8
Menzel, D. H. 1962, Selected Papers on Physical Processes in Ionized Plasmas, ed. D. H. Menzel (New York: Dover)
Nomoto, K., Suzuki, T., Shigeyama, T., Kumagai, S., Yamaoka, H., & Saio, H. 1993, Nature, 364, 507
Perelmuter, J.-M. 1993, IAU Circ., No. 5736
Podsiadlowski, Ph., Hsu, J. J. L., Joss, P. C., & Ross, R. R. 1993, Nature, 364, 509
Podsiadlowski, P., Joss, P. A., & Hsu, J. J. L. 1992, ApJ, 391, 246
Ray, A., Singh, K. P., & Sutaria, F. K. 1993, Astrophys. Astron., 14, 53
Richmond, M. W., Treffers, R. R., Filippenko, A. V., Paik, Y., Leibundgut, B., Schulman, E., & Cox, C. V. 1993, AJ, submitted
Schmidt, B. P., et al. 1993, Nature, 364, 600
Schmidt, B. P., et al. 1994, ApJ, in press
Shigeyama, T., Suzuki, T., Kumagai, S., Nomoto, K., Saio, H., & Yamaoka, H. 1994, ApJ, submitted
Suntzeff, N. B., & Bouchet, P. 1990, AJ, 99, 650
Suntzeff, N. B., Phillips, M. M., Depoy, D. L., Elias, J. H., & Walker, A. R. 1991, AJ, 102, 1118
Suzuki, T., Kumagai, S., Shigeyama, T., Nomoto, K., Yamaoka, H., & Saio, H. 1993, ApJ, 419, L73
Swartz, D. A., Clocchiatti, A., Benjamin, R., Lester, D. F., & Wheeler, J. C. 1993, Nature, in press
Szebehely, V. 1967, The Theory of Orbits (New York: Academic)

Teegarden, B. 1993, private communication; see also INTEGRAL, Exploring the Gamma-Ray Frontier, summary of 1992 Phase A Study carried out by the European Space Agency
Utrobin, V. 1993, A&A, submitted
Weaver, T. A., & Woosley, S. E. 1993, Phys. Rep., 227, 65
———. 1994, in preparation
Weaver, T. A., Zimmerman, G. B., & Woosley, S. E. 1978, ApJ, 225, 1021
Wheeler, J. C., & Filippenko, A. V. 1994, in IAU Colloq. 145, Supernovae and Supernova Remnants, ed. R. McCray (Cambridge: Cambridge Univ. Press), in press
Wheeler, J. C., et al. 1993, ApJ, 417, L71
Woosley, S. E. 1991, in Supernovae: The 10th Santa Cruz Summer Workshop in Astronomy and Astrophysics, ed. S. Woosley (New York: Springer-Verlag), 202
Woosley, S. E., & Weaver, T. A. 1982, in Essays in Nuclear Astrophysics, ed. C. A. Barnes, D. D. Clayton, & D. N. Schramm (Cambridge: Cambridge Univ. Press), 377
———. 1988, Phys. Rept., 163, 79
Woosley, S. E., Langer, N., & Weaver, T. A. 1993, ApJ, 411, 823
Woosley, S. E., Pinto, P. A., & Ensman, L. 1988, ApJ, 324, 466
Woosley, S. E., Pinto, P. A., & Hartmann, D. 1989, ApJ, 346, 395
Xu, Y. 1989, Ph.D. thesis, Univ. of Colorado